The transcriptomic response of cells to a drug combination is more than the sum of the responses to the monotherapies

Jennifer E. L. Diaz[1,2,3,9], Mehmet Eren Ahsen[1,4,9],Thomas Schaffter[1,3,5], Xintong Chen[1], Ronald B. Realubit[6,7], Charles Karan[6,7], Andrea Califano[6,8], Bojan Losic[1], Gustavo Stolovitzky[1,3,8,*]

[1]Department of Genetics and Genomics Sciences, Icahn School of Medicine at Mount Sinai, New York, NY

[2]Department of Cell, Developmental, and Regenerative Biology, Icahn School of Medicine at Mount Sinai, New York, NY

[3]IBM Computational Biology Center, IBM Research, Yorktown Heights, NY

[4]Department of Business Administration, University of Illinois at Urbana-Champaign, Champaign, IL

[5]Computational Oncology Group, Sage Bionetworks, Seattle, WA

[6]Department of Systems Biology, Columbia University, New York, NY

[7]Sulzberger Columbia Genome Center, High Throughput Screening Facility, Columbia University Medical Center, New York, NY 10032, USA

[8]Department of Biomedical Informatics, Columbia University, New York, NY, USA

Department of Biochemistry and Molecular Biophysics, Columbia University, New York, NY, USA

Department of Medicine, Columbia University, New York, NY

J.P. Sulzberger Columbia Genome Center, Columbia University, New York, NY, USA.

Herbert Irving Comprehensive Cancer Center, Columbia University, New York, NY, USA

[9]These authors contributed equally.

*Corresponding author

Contact information

Jennifer E. L. Diaz jennifer.long@icahn.mssm.edu

Mehmet Eren Ahsen mehmeteren.ahsen@mssm.edu

Thomas Schaffter tschaff@us.ibm.com

Xintong Chen xintong.chen@icahn.mssm.edu

Ronald B. Realubit rbr2126@cumc.columbia.edu

Chuck Karan ck2389@cumc.columbia.edu

Andrea Califano ac2248@cumc.columbia.edu

Bojan Losic bojan.losic@mssm.edu

Gustavo Stolovitzky gustavo@us.ibm.com

Abstract

Our ability to discover effective drug combinations is limited, in part by insufficient understanding of how the transcriptional response of two monotherapies results in that of their combination. We analyzed matched time course RNAseq profiling of cells treated with single drugs and their combinations and found that the transcriptional signature of the synergistic combination was unique relative to that of either constituent monotherapy. The sequential activation of transcription factors in time in the gene regulatory network was implicated. The nature of this transcriptional cascade suggests that drug synergy may ensue when the transcriptional responses elicited by two unrelated individual drugs are correlated. We used these results as the basis of a simple prediction algorithm attaining an AUROC of 0.77 in the prediction of synergistic drug combinations in an independent dataset.

Introduction

Combination therapy has become increasingly relevant in cancer treatment (1, 2). The complexity of patient-to-patient heterogeneity (3), intratumoral heterogeneity (4) and intracellular pathway dysregulation (5) provides opportunities for combining drugs to induce responses that cannot be achieved with monotherapy. Effective combinations may target multiple pathways (6) or the same pathway (7). They may also reduce the dose of individual drugs, thereby reducing toxicity, or target molecular mechanisms of resistance, thereby prolonging the effective duration of treatment (1, 8-10).

Drug combinations are said to be synergistic if their activity exceeds their expected additive or independent response (3, 11). Synergistic behavior is difficult to predict, so rational combinations may not validate experimentally (12). Hypothesis-driven studies of the mechanisms of synergy and antagonism have focused on a limited set of candidate targets (13, 14). Alternatively, unbiased high-throughput screening assays (15-17) can identify synergistic compounds in a systematic way by assessing cell viability reduction by individual drugs and their combinations. Unfortunately, screening all possible drug-pairs in a panel of N drugs with N_C cell lines at N_D doses requires a large number ($\frac{1}{2} N (N-1) N_D^2 N_C$) of experiments, resulting in high costs that limit the practical reach of this approach. Computational methods to predict synergistic combination candidates are needed to improve the experimental cost-benefit ratio (18, 19).

To address this need, the DREAM (Dialogue on Reverse Engineering Assessment and Methods) Challenges consortium (20) conducted a community-wide competition (the NCI-DREAM Drug Synergy Prediction Challenge) that fostered the development and benchmarking of algorithms for drug synergy prediction. The organizers provided a time course of post-treatment transcriptomics data for each of 14 drugs administered to a lymphoma cell line, and asked participants to predict which of the 91 pairwise combinations would be synergistic (19, 21). One of the key outcomes of the Challenge and other studies was that synergistic drug combinations could be partially predicted from the transcriptomics of the monotherapies (21, 22). The two best-performing teams based their algorithms on the assumption that a concordance of gene expression signatures in drugs with different mechanisms of action often yield synergistic interactions (23, 24). This assumption, while plausible, has little experimental support beyond winning the Challenge. Further, the mechanism behind this phenomenon cannot be ascertained without transcriptomics data from the combination therapy, which was not provided in the Challenge due to cost. We therefore pose a fundamental question that can only be answered with matched monotherapy-combination transcriptomics data: <u>How do two different transcriptomics profiles in cells treated with two different drugs combine to give a new transcriptomics profile when the drugs are applied together?</u> If the combinatorial pattern of two gene expression profiles are different in synergistic versus additive drug combinations, then learning to recognize these patterns may enable us to predict synergistic combinations from the gene expression of monotherapies.

In this paper we explore the relationship between the transcriptional landscape of drug combinations in relation to the profiles of the individual drugs. We performed a systematic, genome-wide analysis of matched time courses of gene expression following perturbation with individual compounds and with their combinations. Deliberately sacrificing breadth for depth, we studied the transcriptional temporal response of an empirically chosen synergistic drug combination, tamoxifen and mefloquine, in breast cancer and prostate cancer cells and compared it to that of additive combinations of withaferin with either tamoxifen or mefloquine. Rather than elucidating specific mechanisms of action for drugs and their combinations, we attempt to examine the transcriptome for molecular indicators of synergy. Our analysis shows that <u>molecular synergy</u> (measured by the number of genes whose expression changes significantly only in the combination), correlates with the Excess over Bliss independence, a

measure of the observed effect of a combination that is greater than the expected effect based on the Bliss model of additivity (11) and increases with time. We used network-based analyses to trace the transcriptional cascade as it unfolds in time in the synergistic combination. We found that transcription factors simultaneously activated by both drugs dominate the cascade. We propose that a pair of drugs with correlated expression signatures is likely to trigger a synergistic effect, even when they target different pathways. We contrast this effect with the correlated, but additive, effect of increasing dose of one drug. Correlation of monotherapies predicted synergistic drug interaction with high accuracy (AUROC=0.77) using the independent DREAM dataset. This study represents a matched monotherapy-combination transcriptomic analysis of synergy, advancing both our understanding of synergy and ability to predict it.

The paper is organized as follows: First, we describe why we chose the monotherapies and combinations used in this paper and identify patterns of gene expression across synergistic and additive combinations. We analyze how those molecular patterns relate to phenotypic synergy and explore synergistic effects on biological processes over time with drug treatment. We then describe our exploration of synergistic effects on gene splicing as an alternative mediator of drug combination effect. Returning to gene expression, we study the mechanism of synergistic gene expression changes by identifying differentially active transcription factors through a transcriptional network and tracing the impact of these transcription factors in a temporal activation cascade. Then we use an independent microarray dataset to verify the hypothesis that correlation between gene expression profiles of monotherapies can be used as an indicator of synergy. Finally, we discuss the structure of the synergistic transcriptional cascade and a plausible conceptual framework for the molecular underpinnings of synergy.

Results

Finding reproducible synergistic and additive combinations

To identify drug-pairs for the detailed time course RNA-seq analysis, we leveraged a pre-existing LINCS drug combination dataset collected at Columbia University (Califano's lab) in the MCF7 cell line, a breast cancer line that is ERalpha positive (25), and the LNCaP cell line, a prostate cancer cell line that is ERbeta positive (26). This dataset had information on all combinations of 99 drugs against 10 different drugs, each combination assessed in a matrix of 4 by 4 doses at 48 hours after drug application. Among these 990 drug combinations, we found

39 synergistic combinations with a maximum Excess over Bliss (EOB) independence over the 4x4 matrix of more than 30%. From these 39, to select synergistic combinations in which both monotherapies played an important role in eliciting synergy, we chose 13 combinations whose constituent monotherapies showed a variety of combinatorial behaviors across the combinations (antagonism, additivity, and synergy in different combinations) for further testing. We re-assessed the synergy of these 13 pairs using a 6 x 6 dose response matrix and found that 9 of the 13 combinations remained synergistic, while 4 exhibited additive or antagonistic responses, which we removed from further study. Tamoxifen appeared in the greatest number (4) of these 9 combinations. Given this data and the known clinical utility of Tamoxifen in ER+ breast cancer (27, 28), we focused on these 4 combinations. Of those 4, we sub-selected the 2 drug pairs with the highest EOB values, Tamoxifen (T) + Mefloquine (M) and T + Withaferin A (W) (EOB = 49 and 43, respectively). We then further measured viability (using the high throughput Cell Titer Glo) and EOB in triplicate experiments using a 10 x 10 dose matrix at 12 hours, 24 hours and 48 hours (Supplementary Files 1-2) after drug treatment, obtaining results that were consistent with the previously found synergy. Note that these two combinations were tested in at least three independent sets of experiments at this point (99x10 screen, 13 combinations, and 2 combinations).

We noted differences in viability, consistent with recent concerns regarding the lack of reproducibility in cell line viability experiments in response to drugs (29, 30), and yet TM remained consistently synergistic despite changes in the viability of its constituent monotherapies. In addition, we noted hormetic dose curves in response to the monotherapies, especially for W (31). These hormetic responses are evidenced by a non-monotonic dose response, with more than 100% viability with respect to control for small doses (about 3 uM for W; Supplementary File 2) or at short times after drug application (T and M at 3 hours, Figure 1C-E). Many factors could contribute to hormesis. For example, it has been observed that efficient use of energetic processes in complex stress responses require biological resources to be deployed by the cell in a timely fashion (temporal hormesis) and at relatively low-doses (dose hormesis) to elicit a protective response (32, 33). The elucidation of these hormetic responses in the context of synergistic interactions could be a fruitful line of research, but goes beyond the scope of this paper.

Finally, we selected doses of these three drugs that synergized in these two combinations at both time points (20 μM T, 10 μM M, 5 μM W) for subsequent study (Supplementary Files 3-4). T and M are also synergistic at 12 and 24 hours as measured by combination index, which quantifies synergy factoring out the dose effects, but T and W are synergistic only at 24 hours (Figure 1-figure supplement 1A). For completeness, we included the combination MW in subsequent studies.

We focused the rest of the study on these three drugs and their combinations (Figure 1A), in an effort to understand how synergy operates at a transcriptomic level (Figure 1B). We studied MCF7 and LNCaP cells under DMSO (vehicle control), T, M and W, and their combinations TM, TW and MW over a 48-hour time course (0, 3, 6, 9, 12, 24 and 48 hours) using nuclei counts as a direct readout of cell viability in relation to DMSO (Figure 1C-H). At these doses, TM (Figure 1C,F) synergistically reduced viability as early as 6 hours, with little effect from T and M individually in MCF7 (Figure 1C) and moderate effect in LNCaP (Figure 1F). The synergistic effect of TW and MW was very small compared to TM in MCF7 (Figure 1D,E) and negligible in LNCaP (Figure 1G,H). In relation to TM, we therefore consider the effects of TW and MW to be additive and dominated by W (Supplementary Files 2,5).

Finally, we wished to study the effect of drug dose on viability, as a combination treatment exposes the cells to more drug than a monotherapy, and this could mimic the effect of increasing drug dose. Additionally, M has been shown to inhibit the function of MDR1, a multi-drug efflux pump (34) and its effect could therefore be simply to increase the intracellular tamoxifen concentration. We analyzed dose curves of T and M as monotherapies (Figure 1-figure supplement 1B). We measured the effect of T alone at 5, 10, 20, 25, and 30 μM, and M alone at 2.5, 5, 10, and 15 μM at 24 hours in MCF7 cells. Viability in 25 and 30 μM T (37.1% and 13.7%) was similar to TM (23%), while viability of cells treated with M at 15 μM was 63.3%. We continued to observe some inter-experiment variability in the efficacy of monotherapies (e.g. T at 20 μM at 24 hours in Figure 1C and Figure 1-figure supplement 1B, the latter measured about two years after the former one). Interpreting 25 μM T as a “sham” combination of 5 and 20 μM T (Figure 1-figure supplement 1B), 30 μM T as a “sham” combination of 10 and 20 μM T, and 15 μM M as a “sham” combination of 5 and 10 μM M, we observed EOBs of 31.5, 53.1, and 17.5 respectively (Supplementary File 6), far lower than the EOB of about 103.9 in TM (Figure 1C). Consistent with the synergistic Combination Index in TM (Figure 1-figure supplement 1A),

this suggests that the synergy we observed is a phenomenon distinct from dose response. To study the transcriptional mechanisms of drug combinations, we collected RNA from the same cultures from which we measured viability at each treatment for RNAseq (except 30 μM T, which caused too much cell death for RNA collection).

Gene expression of drug combinations in relation to monotherapies

For each treatment (in doses and combinations listed above) and time point up to 24 hours we collected samples in triplicate and performed RNAseq studies (Supplementary Files 7-8). The RNAseq data was reliable, with replicates showing a very high concordance and technical noise considerably smaller than the changes in expression observed under different conditions (Figure 1-figure supplement 2A-B). We first examined the gene expression over all treatments and time points in combination experiments (Figure 1I) and variable doses used for the “sham” combinations (Figure 1-figure supplement 2C) in MCF7, and combination experiments in LNCaP (Figure 1-figure supplement 2D). The transcriptional profiles for the monotherapies T and M were more similar to DMSO than TM. The transcriptional profiles for W, TW and MW on the other hand, were similar to each other but different from T, M, TM and DMSO over time. However, gene expression profiles from different doses of the same monotherapy were quite similar, with changes evolving gradually with increasing dose (Figure 1-figure supplement 2C). This pattern mirrors the phenotypic viability profiles (Figure 1C-H, Figure 1-figure supplement 1B). Figure 1J shows a two-dimensional principal component analysis (PCA) of the transcriptional data from the combination and dose experiments in MCF7. The data for T and M monotherapies, from both the combination experiments and the dose experiments, localize slightly but distinctly above DMSO. However, their TM combination is farther from DMSO than T or M but in the same vertical plane. The PCA representation of W progresses in an almost horizontal direction, with TW and MW co-localizing with W, which dominates the combination. Therefore the 2-dimensional PCA representation of the transcriptomes after treatment suggests orthogonal synergistic and additive directions. The PCA representation of the gene expression from treated LNCaP cells indicates very similar dynamics in this distinct cell line (Figure 1-figure supplement 2E).

We next examined differential expression relative to DMSO. The high concordance of replicates allowed for clear detection of differentially expressed genes (DEGs) in different conditions (Figure 2-figure supplement 1A). To determine DEGs in MCF7, we selected a false discovery

rate (FDR) cutoff at which the only DEGs at time 0 (~30 min post-treatment; see Methods) over all treatments are well-known immediate early genes (35, 36; Table). We then used this cutoff across all time points and treatments of the fixed dose experiments. To achieve consistency in our treatment of the variable dose experiments which were done separately and with fewer replicates, we chose an FDR cutoff resulting in approximately the same number of DEGs in M 10 μM and T 20 μM (Figure 2-figure supplement 1B; see Methods). In LNCaP, we selected a false discovery rate (FDR) cutoff at which there were no DEGs at time 0, as we noticed no differentially expressed immediate early genes in this case (see Methods). We then quantified and examined the properties of DEGs in monotherapies and their combinations. The number of DEGs in MCF7 cells treated with TM, W, MW, and TW were 1 to 2 orders of magnitude greater than that of treatments with T and M (Figure 2A-C). We evaluated the presence of *synergistically expressed genes (SEGs)*, which we define as *genes that are differentially expressed in a combination therapy but not in either of the constituent monotherapies*. Approximately 90% of DEGs in MCF7 cells treated with TM are synergistic, and not differentially expressed in either T or M alone (Figure 2A) at any time point. To test for artifacts related to the chosen FDR cutoff, we calculated the percentage of SEGs over different FDR thresholds and observed that the general trend is independent of the specific cutoff (Figure 2-figure supplement 1C-D). In contrast, most DEGs in treatments TW and MW were also differentially expressed in W (Figure 2B-C). These molecular signatures parallel the effect of these drugs on viability (Figure 1C-E), reflecting the overall synergistic character of TM, and a mostly additive dominant effect of W. In LNCaP cells, we observed a similar effect of TM: more than 75% of DEGs are SEGs at any time point (Figure 2-figure supplement 2A). However, we observed that when LNCaP cells were treated with TW or MW, more than a quarter of DEGs were SEGs at any time point, and more than half at 12 and 24 hours (Figure 2-figure supplement 2B-C); in comparison, in MCF7 cells treated with MW or TW, less than a quarter of DEGs were SEGs at nearly every time point (Figure 2B-C). This highlights the ability of different cells to respond differently to drugs, and we explore it further in the next section. Interestingly, across both cell lines and including the pairs in our dose experiments, the number of SEGs correlates well (Pearson $r=0.63$, $p=0.000044$; Spearman $r_s=0.59$, $p=0.00013$) with EOB for all treatments and time points, (Figure 2D). The number of SEGs and the EOB of T 25 μM and M 15 μM are similar to TW and MW and considerably smaller than TM, consistent with the interpretations that behavior of TW and MW represent additivity, and that the molecular and phenotypic synergy of TM transcends the expected behavior of a simple increase in dose.

Finally, we also observed a significant relationship between the EOB of a combination and the correlation of the transcriptional profiles of the constituent monotherapies (Figure 2E; see Methods). Conversely, the monotherapy pairs from our dose experiments (i.e. T 5 and 20 μM, M 5 and 10 μM) had high correlation as expected, but low EOB. For this reason, when including the dose experiments, the direct correlation between EOB and the correlation of transcriptional profiles (see Methods) is not significant (Pearson r=0.31, p=0.068; Spearman r_s=0.28, p=0.097). When we removed these sham combination pairs from the dose experiments, we observed a significant relationship between EOB and correlation of transcriptional profiles (Pearson r=0.59, p=0.00064; Spearman r_s=0.54, p=0.019). This result suggests that correlated transcriptional profiles of two distinct drugs may be important in defining synergy. Further study in other contexts would be necessary to generalize this hypothesis. The possible nature of correlation as a necessary but not sufficient condition for synergy will be discussed further in a later section.

Critical cancer pathways are synergistically enriched

We checked for enrichment of gene sets associated with specific biological processes. Candidate gene sets were selected from gene-set libraries retrieved from the Enrichr tool (37, 38), pathways implicated in the hallmarks of cancer (39), and likely drug targets of T and M (see Methods). Figure 3 shows the biological processes that are enriched in at least one of the subgroups of DEGs in MCF7 cells under treatment with T, M, TM, as well as in the set T∪M, the union of DEGs under T or M, which represents the expected DEGs if T and M acted additively. If T and M act synergistically, we expect that the set of DEGs in TM should be enriched in more functional classes than T∪M. Implicated biological processes fell into three classes: 1) endoplasmic reticulum stress, estrogen signaling, and kinase activity were enriched in both TM and monotherapies; 2) apoptosis, toll-like receptor and cytokine signaling, immunity, transcription, metabolic processes, and autophagy were markedly more enriched in the combination TM than in either monotherapy or T∪M, an effect no recapitulated by increasing monotherapy dose at 24 hours; and 3) downregulation of the cell cycle was present in both the combination and monotherapies at 12 and 24 hours, but began to occur much earlier in the combination (Figure 3). Classes 2 and 3 appear to be synergistically affected in TM but were not synergistic in either TW or MW (Figure 3-figure supplement 1A).

We also interrogated the dysregulated genes in the treated LNCaP cells by the same procedure. As more SEGs had appeared in LNCaP cells treated with MW and TW than in MCF7, especially at 12 and 24 hours (Figure 2D), we compared the synergistically enriched gene sets in LNCaP cells for TM, TW, and MW (Figure 3-figure supplement 1B). A few biological processes, such as autophagy, were synergistically enriched in all three combinations. Gene sets for which we observed differences between the combinations fell into two broad groups: synergistically enriched more in W combinations (W-enriched) or synergistically enriched more in TM (TM-enriched). The W-enriched gene sets included two main classes: 1) cholesterol biosynthesis and metabolism was only synergistically upregulated in MW and 2) rRNA and ncRNA processing was synergistically upregulated only in TW at 24 hours, while tRNA and mitochondrial RNA processing was synergistically downregulated at some time points in both TW and MW. TM-enriched gene sets fell into three classes: 1) temporal differences: endoplasmic reticulum stress was upregulated at earlier time points in TM than in the monotherapies, whereas it was similarly enriched in W, TW, and MW at all time points except 24 hours, and intrinsic apoptosis in response to ER stress was upregulated initially in W, TW, and MW followed by normalization over time, whereas in TM it was synergistically upregulated in an increasing manner over time; 2) certain metabolic processes (generation of precursor metabolites and energy, cofactors, amino acids, and sulfur) were synergistically downregulated only in TM; and 3) genes that are repressed by estrogen receptor were synergistically upregulated only in TM. We hypothesize that the W-enriched classes represent mechanisms by which LNCaP cells counter the effects of the drug combinations and evade cell death, whereas TM-enriched gene sets, particularly class 2, may represent gene sets that function as harbingers of phenotypic synergy, distinguishing synergistic drug combinations from combinations whose effects can be resisted by cells.

Finally, we assessed for enrichment in phospholipidosis (PLD) in both cell lines. Research has shown that drugs that induce lysosomal stress and lipid accumulation (phospholipidosis), including tamoxifen and mefloquine, tend to exhibit similar transcriptional profiles (40-42). We quantified enrichment in several types of gene sets with a focus on PLD (40; see Methods): cellular components, including in the top 20 gene ontology gene sets associated with PLD; a PLD gene signature (provided by authors of 40); and a set of the gene targets of two transcription factors (TFE3 and TFEB) shown to be involved in lysosomal stress. We found that some PLD-associated cellular components are synergistically affected in TM, including the

lysosome, Golgi, mitochondrion, nucleus, and nucleolus. PLD was highly enriched in all treatments in both cell lines (Figure 3-figure supplement 2), indicating a generalized toxicity-associated effects of treatment. We studied the role that PLD might play in the high correlation between monotherapies in our experiments. We found that the relationship between correlation and EOB (excluding dose experiments) holds even when PLD genes were removed (r=0.59, p=0.00068; Spearman r_s=0.55, p=0.0017). Furthermore, we found that genes in the PLD signature accounted for a small proportion of DEGs in all treatments (data not shown), and as a result the correlation between monotherapies is nearly identical whether we include or exclude the PLD signature genes. (A plot of the correlation between monotherapies including the PLD signature genes vs the correlation between monotherapies excluding the PLD signature genes yielded an almost perfect identity line with: r=0.9999, p=1e-65; Spearman r_s=0.9995, p=2e-52). Finally, enrichment of the PLD signature gene set in TM was only slightly greater than in TUM (Figure 3-figure supplement 2A for MCF7, Figure 3-figure supplement 2C for LnCAP), indicating at best mild synergy in PLD signature genes. These results show that PLD plays a role in the treatments considered here and that some transcriptional similarity between the monotherapies may be associated with PLD. However, PLD is one of many cellular processes triggered by the drug treatments considered here, and it accounts only in a small part for the transcriptional correlation and synergistic gene expression we observed.

Co-expressed genes show a synergistic temporal pattern

We studied temporal patterns of drug response. We used k-means clustering (see Methods) to identify co-expressed genes with similar time evolution in T, M and TM (Source Data File 7). This unsupervised clustering method identified four distinct temporal patterns (Figure 4A): 1) upregulated in TM (2253 genes), 2) strongly upregulated in TM (421 genes), 3) downregulated in TM (1709 genes), 4) strongly downregulated in TM (718 genes). In each cluster, the average differential expression observed in the combination TM was significantly stronger than that in T + M, in which the (log) expression in T and M are added. The trajectory over time for most genes is monotonic and saturates at 9 hours. However, we also tested for genes whose trajectories were significantly different in TM than T and M (data not shown). A minority of genes in each cluster exhibited unique temporal profiles in TM, including mixed transient and monotonic behavior, suggesting the existence of temporal synergy (e.g., Figure 4B).

We then assessed these gene classes for enrichment in biological processes (Figure 4C). Consistent with enrichment of these processes at each time point (Figure 3), upregulated genes were enriched in endoplasmic reticulum stress (clusters 1-2), and downregulated genes were enriched in cell cycle and metabolic processes (clusters 3-4). In addition, apoptosis and downregulated targets of estrogen were enriched in genes strongly upregulated in TM (cluster 2), highlighting synergistic properties. Metabolic processes and the cell cycle were distinguished by clusters 3 and 4, highlighting the biological significance of the degree of downregulation. Finally, the genes with significantly different trajectories in TM account for a small but distinct subset of these synergistic biological processes (data not shown). Together, these data indicate that monotonic dysregulation dominates gene behavior and triggers important biological processes, which implies that the early transcriptional responses might be sufficient to predict synergy.

Synergistically spliced and expressed genes are different

We studied splicing by examining the relative exon usage for each gene. Combination treatment TM induced unique patterns of relative exon usage, compared to DMSO, T, and M. For example, many exons were less used in TM, consistent with an exon skipping modality of alternative splicing (Figure 5). As with differential gene expression, most differentially spliced genes in TM were synergistic, i.e., not differentially spliced in either monotherapy (Figure 6-figure supplement 1A). This was not the case with the combinations involving W (Figure 6-figure supplement 1B-C) where the differentially spliced genes in MW and TW had substantial overlap with the differentially spliced genes in W. However, these synergistically spliced genes were generally distinct from the SEGs (Figure 6A and Figure 6-figure supplement 1D-F). Despite this distinction, the number of synergistically spliced genes correlated with the EOB score (Pearson $r=0.73$, $p=0.002$; Spearman $r_s=0.75$, $p=0.0017$) over all treatments and time points (Figure 6B), as with the SEGs (Figure 2D). These data suggest that expression and splicing represent two separate mechanisms driving phenotypic synergy.

Synergistic activation of transcription factors

We next examined how regulation of the transcriptome can be affected synergistically. We focused on the MCF7 data for this analysis as we were able leverage a robust pre-existing

MCF7-specific transcriptional network (43). Research has shown that the activity of a transcription factor (TF) can be inferred from expression of its targets (44, 45). Because activity of a TF may be affected in many ways, including post-translational modification, co-factor binding, and cellular localization, this approach is a more robust measure of activity beyond simply measuring expression of the TF itself. We utilized a conservative method for this analysis that distinguishes positive effector and negative effector (repressor) functions of a TF (Figure 7-figure supplement 1A; see Methods). Of the 1,101 TFs studied, most of the differentially active (DA) ones were uniquely active as a positive effector, suggesting that much of the response to these drugs is the result of upregulation of genes, and positive TF-gene interactions (Figure 7-figure supplement 2 A-B).

Similarly to the differential expression and differential splicing results, most differentially active transcription factors (DATFs) in TM were not DA in the monotherapies T and M (Figure 7A). Conversely, most DATFs in TW and MW were also DA in W (Figure 7B-C). The majority of DATFs over all treatments and times were produced from genes that were differentially expressed or differentially spliced (Figure 8A). However, some instances of DATFs did not correspond to differential expression or splicing and may represent TFs that become DA by mechanisms not captured by RNA-seq, including some that have a known connection to cancer treatment or to biological processes identified in Figure 3. For example, ATF4, one of the top DATFs in TM, is not differentially expressed nor spliced, and is a key regulator of the response to endoplasmic reticulum stress (46).

Examining TF activity over time, we found that most DATFs, once DA, tend to remain so at later time points. This time course in TM was distinct from T and M (Figure 8B), whereas those of W, TW, and MW were very similar (Figure 8-figure supplement 1). In addition, the patterns of differential TF activity were remarkably similar in T and M, and in fact these two monotherapies had a higher correlation in differential activity values of significant TFs than either of the W pairings (Spearman r at 12 hours: 0.8 in T and M, 0.1 in T and W, 0.4 in M and W), echoing the differential expression data (Figure 2E). Using the set of DATFs in at least one time point in T, M, and TM (Figure 8B), we examined the enrichment of their target sets in the temporal gene clusters identified by k-means clustering (Figure 4). The genes in each cluster are significantly enriched in distinct TF target sets, suggesting that the temporal patterns are regulated by different TFs (Figure 8C).

TF activation in monotherapies can account for synergistic gene expression in combinations via a TF activation cascade

We next asked how the combination of T and M gives rise to the synergistic activity of TFs in TM in MCF7. We hypothesized that DATFs in T and/or M could alter the activity of other TFs when both drugs are administered together. We examined two possible mechanisms by which this could happen in combination TM. First, *distinct* DATFs in each monotherapy may converge as regulators of other TFs when the two monotherapies are combined. This is an “AND” model for the activation of a TF, in that both TFs need to be active in the combination for the activation of their targets. Alternatively, *the same* DATF in T and M may be more strongly DA in TM due to the combined activating effects of the two monotherapies. This dose enhancement mechanism in the combination will be called the “double-down” model. We also assessed TFs that are linked through the MCF7 transcriptional network to those explained by these AND and double-down models in the same time point, as multiple rounds of transcriptional effects could occur within 3 hours (Figure 9-figure supplement 1; 47).

We examined the potential effect of these two mechanisms on synergistic TFs and SEGs (Figure 9 and Figure 9-figure supplement 1). At each time point, we identified the synergistic TFs that could have resulted from the AND mechanism (converging red and blue arrows in Figure 9), and the double-down mechanism (magenta arrows). At time 3 hours, for example, there are two TFs that are active in T, M, and TM: *MYC* and *KLF10*. These TFs are connected through the network to 9 TFs (Figure 9) active in TM (but not in T or M). These TFs are in turn connected to 16 additional TFs (Figure 9-figure supplement 1) active in TM (but not in T or M), giving a total of 25 TFs accounting for 42% of all synergistic TFs. Because there was no active TF in T alone, there was no AND mechanism at work. At 9 hours, 2 new TFs become active in T alone, 18 in M alone and 3 in both T and M, accounting for 12 new synergistic TFs: 6 via the AND mechanism (purple), 4 via the double-down mechanism, and 2 additional TFs due to a combination of AND and double-down models (Figure 9-figure supplement 1). At each time point after 3 hours we identified TFs connected to TFs identified at the immediately previous time point (vertical arrows). Over all time points, the double-down model alone can explain 83 synergistic TFs, the AND model only explains 12 TFs, and mixed AND and double-down explain 4. In total, this cascade of TF activation accounted for the majority of synergistic TFs at all time points, with 88% of the synergistic TFs at 24 hours explained by the cascade of activation

initiated by the 2 TFs activated at 3 hours in both T and M. The number of TFs arising from TFs synergistically activated at previous time points was substantial and accounted for the majority of identified TFs after 3 hours.

We next asked how the AND and double-down mechanisms, along with the activation of synergistic TFs resulting from them, affected the larger group of SEGs. Here, we identified genes potentially affected by the AND and double-down mechanisms, as well as those connected to the newly identified TFs at the current and previous time point. At 3 hours, 29 SEGs can be ascribed to the double-down mechanism, and 146 are direct targets of the newly explained TFs (Figure 9). In all, this accounts for 175 (46%) of all SEGs. By 12 and 24 hours, the vast majority (78% and 79% respectively) of SEGs were explained by this cascade. Together, these data suggest that T and M act in concert, mostly through the double-down mechanism, to trigger a transcriptional cascade that results in substantial differential activation of synergistic TFs and genes not seen in either monotherapy.

Predicting drug synergy in an independent dataset

We have observed that correlation of gene expression of monotherapies is associated with phenotypic synergy in MCF7 cells treated with our three combinations (Figure 2E). We next wished to test the generalizability of this association by leveraging the independent DREAM Challenge dataset (19), which utilized microarray data from LY3 DLBCL cells treated. Of the 91 drug pairs, 81% of the synergistic combinations have correlation > 0.3 (Figure 10A). Indeed the average correlation for the pairs with EOB > 2.5 (at which the average EOB in three replicates is larger than zero by more than the standard error) is 0.48 which is statistically significantly (t-test p=1.0E-8) larger than the average correlation of 0.3 for pairs with EOB < -2.5. As in our dataset, monotherapy correlation is associated with EOB (Pearson r=0.27, p=0.009; Spearman r_s=0.27, p=0.01).

As previous work has suggested that transcriptionally similar, but structurally different drugs are associated with PLD (40), we assessed enrichment of the PLD gene signature in the DREAM drug pairs, using the union of the DEGs in either monotherapy for each pair. We found that monotherapy correlation is associated with enrichment in PLD (Pearson r=0.28, p=0.008; Spearman r_s=0.27, p=0.009), confirming prior studies. However, we found no association between enrichment in PLD and EOB (Pearson r=-0.10, p=0.36; Spearman r_s=-0.12, p=0.26).

Additionally, as in our own dataset, the relationship between correlation and EOB holds when PLD genes are removed (Pearson r=0.27, p=0.009; Spearman r_s=0.28, p=0.008). These data suggest that correlation of monotherapies may be a necessary, but not sufficient, condition for synergy. Additionally, gene expression in processes such as PLD may be significant, but additive or mildly synergistic in nature (Figure 3-figure supplement 2), and thus may play a role in the non-synergistic outcomes of correlated monotherapies. (Figure 10B) outlines a conceptual framework for this relationship. However, we note that unlike in our dataset that is more limited in breadth, correlation of monotherapies and EOB are not linearly correlated in the DREAM data (Figure 10A). Furthermore, any relationship between PLD and either molecular or phenotypic synergy has not been explicitly examined in prior studies. Therefore, validation of our findings in multiple contexts is needed to generalize these claims.

Finally, we used the Pearson correlation between DEGs in monotherapies to predict synergy of their combination and compared these results to those of DIGRE, the best performing method in the DREAM Challenge (24), in predicting the 16 synergistic drug pairs out of the total 91 pairs in the DREAM dataset (see Methods). Correlation outperforms DIGRE in AUROC (Figure 10C) and AUPR (Figure 10D), with Bayes factors (48) of 3.79 and 34.71, indicating statistical significance with Bayes factors >3 (49). It is interesting that simply computing the correlation coefficient between the transcriptomic response of cells to each of a pair of drugs produces a robust predictor of the synergy of the combination.

Discussion

In this paper we studied gene expression data taken from cells after treatment with monotherapies and their combinations in a detailed time course analysis, to elucidate the transcriptional mechanisms underlying synergistic drug interactions. We studied three drug combinations on MCF7 breast cancer cells and LnCAP prostate cancer cells: tamoxifen and mefloquine (TM), tamoxifen and withaferin (TW), and mefloquine and withaferin (MW). Of these three combinations, TM was dramatically synergistic (Figure 1C,F). A mechanistic rationale for its efficacy is not obvious from the known target processes of T (estrogen signaling; 50) and M (autophagy; 51). However, the effect of M on estrogen receptor target gene sets (Figure 3 for MCF7, Figure 3-figure supplement 1B for LnCAP) indicates a moderate anti-estrogen effect, akin to the effect of recently developed novel quinolone derivative estrogen receptor antagonists (52-54). This suggests an unexpected overlap in the targets of T and M, even if estrogen

receptor represents an “off-target” of M, rather than a primary target, and may contribute in part to the high gene expression correlation we observed. Although these data, the *in vitro* synergy of TM, and mouse *in vivo* response to chloroquine and tamoxifen (55) makes this combination an attractive candidate for further study, we are not aware of clinical studies on it in cancer. The experiments required to validate the targets and synergistic mechanisms of TM and its *in vivo* effect would be beyond the scope of this study. Our aim was to shed light on the transcriptional response of the combination in terms of the monotherapies.

We have explored the regulation of synergy in MCF7 by integrating our gene expression data with an MCF7-specific transcriptional network, which allowed us to estimate the differential activation of TFs. Possibly due to overlapping target sets of T and M, we find that TF activity is remarkably correlated between T and M treatments at all time points, resulting in a considerably higher correlation in gene expression for this drug pair than the other two drug pairs we examined. This correlated TF activation in response to T and M results in a “double-down” effect in the combination, where a TF activated by both drugs is reinforced in its activation in the combination at early time points, beginning with early response TFs MYC and KLF10 (36). *MYC* is a proto-oncogene present in a low-level amplification in MCF-7 cells, likely functioning as an oncogene (56-58). It has been implicated in regulating the unfolded protein response after prolonged tamoxifen treatment (59), suggesting it may play a role in the ER stress we observed in response to tamoxifen treatment. Conversely, *KLF10* is a tumor suppressor that represses *MYC* expression in healthy cells and is involved in repressing proliferation and inducing apoptosis (60). It may therefore act to check unregulated *MYC* expression and facilitate the induction of apoptosis.

The action of these TFs triggers a transcriptional cascade that expands over time and results in the emergence of a massive number of SEGs (DEGs in the combination but not in either monotherapy) not recapitulated by increasing monotherapy dose. We found that a high number of SEGs is strongly associated with the synergistic combination in MCF7, whereas all combinations produced SEGs in LNCaP, only one of which resulted in phenotypic synergy (Figure 2D). The data suggest that SEGs are a sensitive, but not specific, molecular indicator of synergistic processes in the combination, which in the case of TM includes pro-cell death processes. This phenomenon is distinct from the relationship between differential expression

and cell death, which can reflect processes triggered by single agents, unrelated to the behavior of combinations.

The SEGs resulting from this cascade contribute to specific biological processes that are likely responsible for the killing effect of the combination TM, including activation of intrinsic apoptosis in response to endoplasmic reticulum stress and cell cycle arrest. While T promotes apoptosis (61), cells are rescued in part by the pro-survival activation of autophagy (62), which degrades and recycles metabolites and other cellular constituents including depolarizing mitochondria (63). Autophagy is enriched in T treated cells, likely in response to the unfolded protein response triggered by ER stress (63; Figure 3, Figure 3-figure supplement 1B), and perhaps accounting for the poor efficacy of T in the first 24 hours (Figure 1C,F). Research indicates that treatment with M (an antimalarial agent) alters regulation of autophagy in a cell-type specific manner (51, 64, 65). This effect may compromise mitochondrial recycling resulting in lower ATP levels (66).

When treating cells with T and M simultaneously, we expect that the pro-survival effects of the autophagy pathway will be abrogated by M, leading to a synergistic shutdown of metabolic processes, and cell death by apoptosis (67). Indeed, we observed synergistic changes in apoptosis and autophagy in both cell lines upon TM treatment (Figure 3, Figure 3-figure supplement 1B). The large numbers of SEGs we observed in all combinations in LNCaP cells (Figure 2D) allowed us to study the distinction between SEGs in combinations with phenotypic synergy and those without. W, TW, and MW all quickly downregulated biogenesis of RNA and protein, TW upregulated RNA metabolism, and MW upregulated cholesterol metabolism, which may be physiologic responses to ER stress (68, 69), whereas cells in TM regulated these processes more slowly. Perhaps through the combined protective effects of synergistically upregulating autophagy and downregulating biogenesis, cells treated with the W combinations were able to recover from an initial upregulation of intrinsic apoptosis in response to ER stress. In TM, however, the upregulation of autophagy and downregulation of biogenesis were not as robust, and cells gradually and synergistically downregulated metabolism and upregulated intrinsic apoptosis in response to ER stress (Figure 3-figure supplement 1A). These data indicate that drug combinations can induce SEGs that represent either protective responses or cell death, only the latter of which results in phenotypic synergy. This suggests SEGs are a necessary, but not sufficient, condition for synergy.

In MCF7, cell competition induced by varying levels of the synergistically active TF MYC may activate the synergistically upregulated *IRAK2* and its NFkB effectors (*NFKB1*, *CASP8*, and *NFKBIA* are upregulated in TM), triggering apoptosis in the less fit cells (70). Cells that are dying or undergoing ER stress produce damage-associated molecular patterns (71), which activate *TLR3* signaling through a *MYD88*-independent (*MYD88* and its adaptor *IRAK1* are synergistically downregulated in TM) and *TRIF*-mediated pathway leading to the activation pro-inflammatory NFkB signaling (72). All these biological processes (*TLR3* signaling, *MYD88*-independent and *TRIF*-dependent regulation of cytokines, NFkB signaling) are synergistically enriched in TM. The crosstalk between cellular stress response and innate immune signaling likely accounts for the enrichment of immunity functional classes (73). The emergence of these synergistic functional gene classes was not recapitulated by increasing monotherapy dose (Figure 3). Rather, they are unique to the combination. This suggests that a focus on known targets of monotherapies is insufficient to predict the effects of combinations.

The utilization of RNAseq technology allowed us to examine synergistic effects on RNA splicing, an approach not previously available to studies of synergy that used microarrays. Splicing may alter the proteomic function by adding or deleting a key regulatory protein domain (74). We found considerable activation of alternatively spliced genes in MCF7 cells in the combination TM but not in either monotherapy. It is of interest that these alternatively spliced genes typically were not differentially expressed themselves. We found that like synergistic gene expression, synergistic splicing was dramatically higher in TM than TW and MW. This likely represents a distinct molecular mechanism of synergy (Figure 6), consistent with previous work on transcription and alternative splicing (75). Exploring this preliminary evidence further, for example with long-read technology (74), may reveal a stronger role for isoform switching in drug response than previously thought.

While some previous research has indicated that synergy is context-specific (10, 76, 77), the DREAM Challenge results suggested that similarity of monotherapies is associated with synergy. We observed this phenomenon in the present study in an independent context, measuring similarity by transcriptome correlation, and validated the finding in the DREAM dataset (Figure 10A). We also examined the role of the previously identified relationship

between PLD and similarity of monotherapy transcriptomes (40), validating this relationship but finding that it does not appear to mediate the effect of correlation on synergy.

Our findings have led us to hypothesize about general features of synergy. Our analysis indicates that while all synergistic combinations have correlated monotherapies, the converse is not necessarily true: some drug pairs are correlated in gene expression, but do not generate a synergistic effect. Indeed, when we combine two doses of the same drug (sham combination), whose gene expression profiles are by nature correlated, this does not result in appreciably high EOB (Figure 2E). This suggests that the mechanism whereby synergy ensues from transcriptionally correlated but not identical drugs has to include the AND type of activation even if the double-down mechanism is dominant, as was the case in the transcriptional cascade of (Figure 9). Correlated monotherapies and SEGs appear to be related phenomena that are required for synergy, but insufficient to generate it in all cases. We propose a conceptual framework for the relationship between monotherapy correlation, number of synergistically expressed and spliced genes and the activation of key pathways to account for these findings in Figure 10B. In this framework, correlated monotherapies can act through the “double-down” mechanism generating a transcriptional cascade resulting in expression of many SEGs. We hypothesize that where SEGs are enriched in pro-cell death genes as in our MCF7 data (Figure 3), this leads to phenotypic synergy. However, there may exist correlated drug pairs that generate only additive gene expression in biological processes such as PLD, or where SEGs appear but represent pro-survival programs or processes unrelated to cell viability, such as in LNCaP cells treated with TW or MW (Figure 3-figure supplement 2C). Under these conditions, correlated monotherapies would not result in a synergistic combination. Further studies on this theory in other contexts are necessary. However to our knowledge, only the data presented here and the DREAM dataset we used has matched post-treatment expression and viability data, limiting our ability to validate our findings regarding the gene expression patterns associated with synergy.

We have shown that gene expression correlation can be used to predict synergy with higher accuracy than the best performing algorithm in the DREAM Challenge (Figure 10C-D). As the DREAM dataset consists of microarrays in a lymphoma cell line, the importance of correlation appears to be independent of both cell type and gene expression measurement technology. Additionally, the monotonicity of our gene expression time course in the combination (Figure 4A)

indicates gene expression at later time points can be predicted from earlier ones, and synergy can therefore be predicted from a single time point. These rules of synergy could therefore be used as the basis for *in silico* screening of drug pairs for synergy using existing gene expression datasets. This approach may be an efficient and cost-effective precursor to preclinical studies of drug synergy.

Acknowledgements

We thank Mukesh Bansal, James Bieker, Ross Cagan, Jing He, and Carlos Villacorta for useful discussions. We thank the authors of Sirci et al. for sharing the PLD gene signature. We also acknowledge support to Jennifer Diaz from NIH grants T32 GM007280 and NIH-U54OD020353, and to Andrea Califano from U54 CA209997 (Cancer Systems Biology Consortium), S10 OD012351 and S10 OD021764 (Shared Instrument Grants). Research reported in this paper was supported by the Office of Research Infrastructure of the National Institutes of Health under award numbers S10OD018522 and S10OD026880. The content is solely the responsibility of the authors and does not necessarily represent the official views of the National Institutes of Health.

Declaration of Interests

Dr. Califano is founder, equity holder, consultant, and director of DarwinHealth Inc., a company that has licensed some of the algorithms used in this manuscript from Columbia University. Columbia University is also an equity holder in DarwinHealth Inc.

The other authors have no competing interests to declare.

Data and Code

Raw RNAseq data is available from the Gene Expression Omnibus under accession GSE149428 (ncbi.nlm.nih.gov/geo/query/acc.cgi?acc=GSE149428).

Code is available at github.com/jennifereldiaz/drug-synergy.

Methods

Key Resources Table

Reagent type (species) or resource	Designation	Source or reference	Identifiers	Additional information
cell line (*Homo-sapiens*)	MCF7	American Type Culture Collection	Cat No. HTB-22	RRID:CVCL_0031
cell line (*Homo-sapiens*)	LNCaP	American Type Culture Collection	Cat No. CRL-1740	RRID:CVCL_1379
chemical compound, drug	Withaferin A	Enzo Life Sciences	Cat No. BML-CT104-0010	
chemical compound, drug	Mefloquine hydrochloride	Sigma-Aldrich	Cat No. M2319-100MG	
chemical compound, drug	Tamoxifen citrate	Tocris Bioscience	Cat No. 0999	

Cell Culture

MCF-7 (ATCC HTB-22) cells were obtained from ATCC. Cells were cultured according to manufacturer's recommendations in ATCC-formulated Eagle's Minimum Essential Medium (Catalog No. 30-2003) with 10% heat-inactivated fetal bovine serum, and 0.01 mg/ml human recombinant insulin. LNCaP cells were purchased from ATCC (Cat No. CRL-1740) and stored in liquid nitrogen until use. Frozen vial was quickly thawed in 37C bath, and then cells were washed from DMSO by spinning in 15ml vial filled with 10mls of PBS. Cells were re-suspended in RPMI media (ATCC, Cat No. 30-2001) supplemented with 10% Fetal Bovine Serum (ATCC, Cat No. 30-2021) and plated into 75cm cell culture flask (Corning, Cat No. 430641). Growth media was changed every 3-4 days. After reaching confluence, cells were split at a ratio 1:6. Cultures were tested for mycoplasma periodically using MycoAlert (Lonza, Cat No. LT07-701) per manufacturer's instructions.

To split, media was removed, cells were washed with PBS, and trypsin-EDTA mix was added for 5 min. After detachment, cells were washed with growth media, collected into 50ml vial, spin down at 1000RPM, suspended in fresh media and plated into 75cm flasks. Cells were treated

with Withaferin A (Enzo Life Sciences BML-CT104-0010), Mefloquine hydrochloride (Sigma-Aldrich M2319-100MG) or Tamoxifen citrate (Tocris 0999) in 0.3% DMSO for the viability time courses (Figure 1C-H, Supplementary Files 4-5) or 0.4% DMSO for dose-response curves (Figure 1-figure supplement 1 B, Supplementary File 6).

Viability

The cells were plated at 10,000 cells per well in a clear bottom black 96w plate (Greiner Cat. No. 655090) and a white 96w plate (Greiner Cat. No. 655083) then they were placed in an incubator. After 24hrs, the plates were removed from the incubator and treated with drugs using the HP D300 Digital Dispenser. After the targeted drug treatment times, 100uL of Cell-Titer-Glo (Promega Corp.) was added to the wells in the white 96w plate and shaken at 500rpm for 5 minutes. The plate was then read by the Perkin Elmer Envision 2104 using an enhanced luminescence protocol to count the number of raw luminescent units per well. For the black clear bottom 96w plates, the plate was spun at 300g for 5 minutes and all the cell media was removed. Methanol was then added at 200ul per well and let sit at room temperature for 15 minutes. The methanol was removed from the wells and 200uL of PBS with Hoechst 33342 nucleic acid stain at a final concentration of 1 uG/mL was then added to the wells. The plates were then imaged with the GE Healthcare IN Cell Analyzer 2000 that is equipped with a CCD camera. The IN Cell Analyzer software was used to count the number of cells detected in each well to calculate the viability. Three replicates were used for the combination experiments and two replicates for the dose experiments.

Calculation of Phenotypic Synergy

Excess over Bliss

Suppose a given drug combination XY inhibits I_{XY} percent of the cells, and the X and Y monotherapies inhibit I_X and I_Y percent of the cells respectively. Note that $V_{XY} = (1 - I_{XY})$ is the viability of the cells, i.e. the percentage of cells that survive after administration of drugs X and Y. Then according to the Bliss model of no interaction between drugs X and Y, the percentage of viable cells in the cell culture treated with combination XY is expected to be $V_X V_Y = (1 - I_X)(1 - I_Y)$. In this calculation, any negative values of I i.e. growth promotion rather than inhibition) are converted to 0. This value is used for the “Bliss Additivity” viability in (Figure 1C-H). As a result, the Excess over Bliss (EOB) independence (78) is given as

$$EOB = 100 * (V_X V_Y - V_{XY}) = 100 * (I_{XY} - (I_X + I_Y - I_X I_Y)),$$

which is the difference between the observed and expected inhibitions. EOB can take any value in the interval [-100,100] and a positive EOB implies synergy, a negative EOB implies antagonism and a value close to zero EOB implies additivity. By propagation of errors, the error of EOB is given as:

$$Error_{EOB} = \sqrt{SEM_X^2(1 + I_Y^2 - 2I_Y) + SEM_Y^2(1 + I_X^2 - 2I_X) + SEM_{XY}^2},$$

where SEM represents the standard error of the mean of the inhibition by a given drug.

Combination Index

Although it is simple to calculate, the EOB described above have some limitations as a measure of synergy. For example, it may classify the combination of a drug with itself as synergistic. An alternative method to quantify synergy uses as a null hypothesis the Loewe additivity model and the associated quantity combination index (CI) (79). The calculation of CI index requires fitting a dose response curve to monotherapies. Therefore, one needs the inhibition values for different doses of monotherapies. As a result, we could only calculate CI for 12, 24 and 48 hours for the TM combination and 12 and 24 hours for the TW combination (Figure 1-figure supplement 1A) and only for viability measured using CellTiter Glo (Supplementary Files 1-2).

Mathematically, the combination index CI is computed as

$$CI = D_{x1}/D_1 + D_{x2}/D_2,$$

where D_1 and D_2 are the required dosage of Drug 1 and Drug 2 to reach certain effect (percentage cell death in this case) when both drugs administered independently. On the other hand, D_{x1} and D_{x2} are the dosage required to attain the same percentage of cell death when both drug are given in combination. Accordingly, a CI<1 suggests synergism, CI =1 suggests additive and CI>1 suggests antagonism between the drugs. We used the ComboSyn software (80) to compute CI.

Processing of the RNA-seq Data

The cells were plated at a density of 8,000 cells per well in a 96 well plate (Greiner Cat. No. 655083) and placed in an incubator. After 24 hours, the plates were removed from the incubator and treated with drugs using the HP D300 Digital Dispenser. The cells were then collected at the targeted time point by removing the media and pipetting 150uL of Qiagen Buffer RLT into each well. The plates were then frozen and stored at -80C. For RNA extraction, the Qiagen RNeasy 96 kit (Cat. No. 74181) was used with the Hamilton ML STAR liquid handling machine equipped with a Vacuubrand 96 well plate vacuum manifold. A Sorvall HT 6 floor centrifuge was used to follow the vacuum/spin version of the RNeasy 96 kit protocol. The samples were treated with DNAse (Rnase-Free Dnase Set Qiagen Cat. No. 79254) during RNA isolation. The RNA samples were then tested for yield and quality with the Bioanalyzer and the Agilent RNA 6000 Pico Kit. The TruSeq Stranded mRNA Library Prep Kit (RS-122-2101/RS-122-2102) was then used to prepare the samples for 30 million reads of single end sequencing (100bp) with the Illumina HiSeq2500. Three replicates were used for the combination experiments and two replicates for the dose experiments (Supplementary File 6).

Generation of Gene Level Count Matrix

We aligned raw reads to hg19 reference genome (UCSC) using the STAR aligner (version 2.4.2a) (81). We used the featureCounts (82) module from subread package (version 1.4.4) to map the aligned reads to genes in the hg19 reference genome, which provided us a gene count matrix with 38 samples and 23228 genes (Supplementary File 8). To reduce the noise due to low count genes, we kept genes with at least one count in at least three control (DMSO) samples at any time point. We normalized the resulting count matrix using Trimmed Mean of M-values (TMM) method (83). We produced log base 2 of count per million (cpm) after adjusting plates as covariates (Source Data Files 1-3). We used the voom package (84) to model the mean variance trend in our data (Figure 1-figure supplement 2A-B).

Differential Expression Analysis

We used the limma (85) pipeline for differential expression analysis to compare treatment with DMSO at respective time points. We corrected the p-values into a false discovery rate (FDR) using BH procedure (86) for multiple testing (Source Data Files 4-6). To determine an appropriate false discovery rate (FDR) cutoff for differential expression, we examined the data for each treatment at time 0. Time “0” represents a treatment of less than 30 minutes, during which drug is added and the cells are then immediately prepared for RNA collection. This time

delay between treatment and RNA collection is likely long enough to allow transcription of immediate early genes. Immediate early gene expression has been shown to be induced within minutes following an external stimulus (35). In the MCF7 combination experiments, the majority of the genes with low p-values at time 0 in our data are known immediate early genes (35, 36). We selected an FDR cutoff of $1.0\,x10^{-18}$ for differential expression (Figure 2-figure supplement 1A), at which the only DEGs at time 0 over all treatments are well-known immediate early genes (Table). For the dose experiments, in which there were two replicates instead of three and thus lower p values, we selected $1.0\,x10^{-5}$ as the lowest FDR cutoff which produced at least as many DEGs as the combination experiments at 24 hours in both T and M (Figure 2-figure supplement 1B). For the LNCaP combination experiments, we selected $1.0x10^{-15}$ as the lowest FDR cutoff for which there were no DEGs at time 0 for any treatments. We did not observe any immediate early genes with low p values at this time point in any treatments in LNCaP.

To calculate monotherapy correlation, for each monotherapy pair, we calculated the Pearson correlation between expression of genes that are differentially expressed in either monotherapy (FDR < 0.1).

Time Course Gene Expression Clustering

To identify the sets of genes that exhibit similar responses to T, M and TM, we clustered their RNA-seq expression profiles. We considered 5101 genes that are differentially expressed for at least one time point (0, 3, 6, 9, 12, or 24 hours) in at least one of the conditions (T, M and TM). First, we computed the mean expression profile of each gene from the expression values of its three replicates A, B, and C ($\log_2$(cpm)). We then normalized the mean expression profiles of the 5101 genes by their respective response to DMSO.

Because we wanted to cluster genes that have similar response in T, M and TM, we joined the vector of normalized expression values in T, M and TM for every gene. Thus, we obtain a vector for each gene that contains 18 values (3 drugs * 6 time points). In order to introduce information about the derivative of the expression profiles, we also joined the delta expression value between each pair of consecutive time point (t3-t0, t6-t3, … t24-t12) for the three conditions. Therefore, the vectors to cluster contains each 33 values.

We applied a k-means clustering algorithms to group the expression vectors into k groups. In order to identify a suitable value for k, we computed the total within-cluster sum of squares for values of k running from 1 to 20. We then selected k equal to 4 clusters as we observed that the gain in information obtained with larger values of k was becoming considerably small. We ran 10'000 times the Hartigan-Wong implementation of the k-means algorithm (87) provided by Matlab with a maximum number of iterations set to 1000 before selecting the partitioning of the vectors that achieved the smallest total within-cluster sum of squares (Source Data File 7).

Gene Set Enrichment Analyses

In each treatment and time point, we separately analyzed the sets of upregulated and downregulated genes for pathways and processes using the built-in Fisher's exact test of the Python package Scipy (88). We assessed enrichment in all gene sets of the GO_Biological_Process database downloaded from the Enrichr (37) library repository (http://amp.pharm.mssm.edu/Enrichr/#stats) and, to assess the known effects of tamoxifen, we used the gene set of estrogen receptor related genes downloaded from the Broad Molecular Signatures Database (89-91). We only performed the test where both gene sets contained at least three genes and the overlap contained at least two genes; if either criterion was not met, no p-value was returned, and a p-value of 1 was used for display in the figures. We then calculated the false discovery rate (FDR)-adjusted p-values using the Benjamini-Hochberg method available in the Python package Statsmodels (92). To select the gene sets that may explain the synergistic gene expression seen in Figure 2 and suggest biological processes involved in the synergistic drug response (Figure 1), we applied four criteria:

1. Synergistic gene sets were defined as those with an FDR less than 0.00001 in at least one time point in TM and less than 0.01 in all time points in TM, but greater than 0.00001 in all time points in TUM or greater than 0.01 in any time point in TUM. TUM refers to the union of genes from T and M that are either upregulated or downregulated.
2. Additive gene sets were defined as those with an FDR less than 0.00001 in at least one time point in TUM and less than 0.01 in all time points in TUM.
3. GO: Keyword searches for terms associated with each of the ten 2011 hallmarks of cancer (39) were performed in the Gene Ontology online database (93). For each hallmark of cancer, the highest level ontology relevant to it was selected, followed by 1-2 levels of children of that ontology that were connected by the relation "is_a", "regulates", "positively_regulates", or

“negatively_regulates”. From the gene sets associated with all these ontologies, those with an FDR less than 0.01 in at least one time point in TM were selected. Five hallmarks remained after applying this filter: metabolism, immunity, cell death (only ‘apoptosis’ was significant), growth, and proliferation (only ‘cell cycle’ was significant).

4. To assess known drug targets including estrogen signaling as a target of tamoxifen (50) and autophagy as a target of mefloquine (51), we included four gene sets related to estrogen signaling from Broad Molecular Signatures Database and any gene sets from the GO Process database containing the words “autophagy” or “estrogen”. Similarly to the hallmarks of cancer, any of these sets with an FDR less than 0.01 in at least one time point in TM were selected.

Together, the results of these four approaches comprise the gene sets shown in Figure 3, Figure 3-figure supplement 1, and Figure 4C.

We employed a similar approach to assess enrichment in cellular components, with a particular focus on the lysosome. We assessed enrichment in all gene sets of the GO_Cellular_Component database downloaded from the Enrichr (37) library repository (http://amp.pharm.mssm.edu/Enrichr/#stats) and, to assess the previously reported lysosomotropic effects of tamoxifen and mefloquine, we used the 250 most upregulated and 250 most downregulated genes in treatment with drugs associated with phospholipidosis, kindly provided by the authors of “Comparing structural and transcriptional drug networks reveals signatures of drug activity and toxicity in transcriptional responses” (40). Based on the findings of the same paper, we also created a gene set made up of the targets of the transcription factors TFEB and TFE3 from our MCF7 network and included it in analysis. The same criteria for statistical testing and false discovery rate procedure as above were used. To select gene sets associated with synergy or additivity, we applied three criteria:

1. Synergistic gene sets were defined as those with an FDR less than 0.00001 in at least one time point in TM and less than 0.01 in all time points in TM, but greater than 0.00001 in all time points in TUM or greater than 0.01 in any time point in TUM. TUM refers to the union of genes from T and M that are either upregulated or downregulated.

2. Additive gene sets were defined as those with an FDR less than 0.00001 in at least one time point in TUM and less than 0.01 in all time points in TUM.

3. Phospholipidosis candidates: We selected the top 20 gene ontology gene sets associated with phospholipidosis in Sirci et al. The gene set “cytoplasmic vesicle” was too large to be included in the Enrichr library, so the gene sets for “cytoplasmic vesicle membrane” and “cytoplasmic vesicle part” were included in its place. From the gene sets associated with these cellular component ontologies as well as the gene sets representing the PLD_up and PLD_down gene signatures and the TFEB_TFE3 transcriptional targets (see above), those with an FDR less than 0.01 in at least one time point in T, M, TUM, or TM were selected. Note that unlike in the hallmarks of cancer analysis, we included any additive gene sets here.

Together, the results of these three approaches comprise the gene sets shown in Figure 3-figure supplement 2.

Generation of Exon Level Count Matrix

We mapped the aligned reads to an in-house flattened exon feature file in hg19 reference genome build using featureCounts from subread package (1.4.4). Flattened exon feature file was generated based on gtf (hg19) downloaded from UCSC with overlapping exons from the same gene removed (Supplementary File 9).

Synergistic Splicing and Exon Expression

We used short read splicing caller: diffSplice (94) in the limma package (version 3.24.3) (85) as framework to detect synergistic spliced genes at each drug combination. We kept exons that have at least one read in at least one sample, and normalized the expressed exon counts using the TMM method (83). For each combination treatment i at a given time point j, we tested synergistic exon expression (SEE) in the generalized linear model of

$$SEE_{ij} = combo_{ij} + DMSO_j - singlet1_{ij} - singlet2_{ij}$$

We performed two statistical tests to detect synergistic exons expression and synergistic spliced genes. For the former, we performed exon level t-statistic test to detect differences between each exon and other exons from the gene, and defined exons with FDR<0.05 as synergistically expressed (the differential exon expression heatmap). For synergistic splicing, we performed Simes test (95) for each gene to test hypothesis of whether usage of exons from the same gene differed, genes with Simes-adjusted p-values<0.05 are defined as synergistically spliced genes.

Generation of the MCF-7 Gene Regulatory Network

The original MCF-7 network has been generated by (43) using the network inference method ARACNE2 (96) and 448 expression profiles for MCF-7 cell line from the connectivity map database (CMAP2; RRID:SCR_015674; 97). The original network includes 20,583 probes, 1,109 of which are transcription factors, and 148,125 regulatory interactions. The interactions predicted by ARACNE2 are directed, unless an interaction is found between two TFs, in which case two edges are included in the list (TF1 to TF2 and TF2 to TF1). To obtain a network at the gene level, we applied a one-to-one HG-U133A probe to gene mapping (97, 98). The mapping file used has last been updated on July 2015 (v3.1.3). We filtered out edges that don't have both nodes present in the mapping list. Finally, in order to determine positive (activation) and negative (repression) interactions, we calculated the Spearman correlation and the corresponding p-value between each TF-target pair in the network. We then corrected the p-values for multiple hypothesis testing and removed edges with low confidence level (FDR <0.05), which gave us the final network with 9,760 genes, 1,101 TFs, and 48,059 regulatory interactions. For each TF in the network, we defined its positively/negatively regulated targets as the genes to which there exist an outgoing edge in the final network with a positive/negative Spearman correlation coefficient.

Quantifying Transcription Factor Activity

To calculate differential activity for each TF in our network, we examined its putative targets as determined by our network. We utilized a conservative method for this analysis that distinguishes positive effector and negative effector (repressor) functions of a TF (Figure 7-figure supplement 1; Source Data File 9). These functions have been found to be distinct (99-101). With this analysis in mind, we performed four comparisons in each treatment and time point:

1. Positively regulated targets of TF and upregulated genes
2. Positively regulated targets of TF and downregulated genes
3. Negatively regulated targets of TF and upregulated genes
4. Negatively regulated targets of TF and downregulated genes

For each of these comparisons, we performed Fisher's exact test as described above for gene set enrichment analysis. This resulted in two p-values for each transcription factor: one for its positive effector function and one for is negative effector function. We then applied the Benjamini/Hochberg false discovery rate (FDR) adjustment to all the resulting p-values over all time points for the treatment.

We used an FDR cutoff of 0.05 to determine differential activity, and we determined the direction of differential activity of each regulon type (Figure 7-figure supplement 1) as follows:

1. Positively regulated targets of TF enriched in upregulated genes → positive effector function activated
2. Positively regulated targets of TF enriched in downregulated genes → positive effector function inactivated
3. Negatively regulated targets of TF enriched in upregulated genes → negative effector function inactivated
4. Negatively regulated targets of TF enriched in downregulated genes → negative effector function activated

We then analyzed each set of two FDR values for the same transcription factor, treatment and time point. If positive and negative effector functions were both activated or both inactivated, the transcription factor was labelled concordant. If one effector function was activated and the other inactivated, the transcription factor was labelled discordant. If only one effector function was differentially active, the transcription factor was labelled unique. For thirty-three transcription factors in 142 cases across all treatments and time points, the same effector function was found to be both activated and inactivated by the above criteria. These nonsensical results were removed from further analysis, and may be due to transcription factors with an unusually large number of targets.

For each of 1,101 transcription factors (43), we identified positively regulated targets and negatively regulated targets using an MCF7-specific transcriptional regulatory network generated by the ARACNe network inference algorithm (96). These two sets represent the distinct targets of each TF's positive effector function and negative effector function. We then assessed the enrichment of each set of targets in the lists of upregulated and downregulated genes in each treatment with respect to DMSO. These enrichment results were used to

determine whether transcription factors were activated or inactivated with respect to DMSO (Figure 7-figure supplement 1). Most transcription factors were uniquely differentially active in their positive effector or negative effector functions, but not both (Figure 7-figure supplement 2A-B).

To account for some transcription factors having very similar sets of targets, we performed Fisher's exact test as above for all possible pairs of transcription factor target sets among those that were significant at each treatment and time point. We then applied the Benjamini/Hochberg FDR adjustment to all the resulting p-values. For each case where the FDR was significant, we then performed Fisher's exact test to assess enrichment of the relevant dysregulated genes in each of three sets: the intersection of the two transcription factor target sets, and each of the target sets individually with the intersection excluded. We then applied the Benjamini/Hochberg FDR adjustment to all the resulting p-values over all cases. Finally, where one effector target set was significantly enriched but the other was not, with their intersection excluded, the significant target set was retained as differentially active, using the original FDR values. All the rest were removed from further analysis.

Graphical Representation of the Transcriptional Cascade

Figure 9 shows the evolution of the active transcriptional network after introducing the two drugs T and M. Figure 9-figure supplement 1 provides a more detailed representation of the mechanisms responsible for the activation of the synergistic TFs. In Figure 9-figure supplement 1, each oval represents the set of TFs that are activated under T, M and/or TM (Source Data File 10): (101) indicates the set of TFs active in T and TM but not in M, (011) indicates the set of TFs active in M and TM but not in T, (111) indicates the set of TF active in T, M and TM. Finally, (001) are TF active in TM but not in T or M. The number next to each oval indicates the number of TFs in that set. In this way we can keep track of the activation of synergistic TFs (001) in TM in terms of the activation of a pair of parent TFs, one in T (101) and one in MM (010), or of one parent TF active also in T and M (111), and doing so at each time point. For example, for the time point at 3h (Figure 9-figure supplement 1), there 2 TFs active in T, M and TM that belong to set (111), 2 TFs active only in M and TM that belong to set (011), and no TF active in T and TM but not in M (101). The middle layer of this representation contains 3 sets of synergistic TFs that are only active in TM, but not in T or M (001) (grey ovals). Each of these three sets include TFs whose regulators (i.e., their own TFs) are at least one TF in (111) (TF activated through the

double-down mechanism: left grey oval in the middle layer), or has two or more parents one in (101) and the other in (011) (TF activated through the AND mechanism: right grey oval in the middle layer), or has three of more parents from sets (101), (111) and (011) (TFs activated through both double down and AND mechanisms: middle grey oval in the middle layer). At 3 h only the double-down mechanism can explain 9 synergistic TFS, which in turn are parents and can explain the activation of 16 additional synergistic TFs, as indicated in the third layer of (Figure 9-figure supplement 1). To the right of the construct we just discussed, there are two more pairs of ovals. The first pair of contains an oval with dashed border, indicating the synergistic TFs that were active at the previous time point (t=0 for 3 h) and the arrow points to the grey oval that indicates how many synergistic TF ative at 3 h can be ascribed to the activation of its regulators in the earlier time point. At 3 hours, both sets are empty. The rightmost pair of ovals, the bottom one represents the set of TFs whose activation can not be explained using any of the above mechanisms. Finally, the diagrams for 12 and 24 hours show additional sets of ovals representing TFs that belong to set (101), (011) and (111) at the previous time point, and that are needed to explain some of the synergistic TFs at the current time point, and whose numbers are indicated in italics in the middle layer of the diagram.

Drug Synergy Prediction in the DREAM Dataset

The DREAM expression matrix was downloaded from Synapse (https://www.synapse.org/#!Synapse:syn2785787). To assess PLD in the DREAM data, we used the aforementioned limma (85) pipeline to calculate differential expression in each treatment compared to DMSO. Then we calculated enrichment of the 500 PLD genes (40; see above) in the genes with fdr < 0.05 in either monotherapy for each drug pair, using Fisher's exact test as described above. For the correlation-based classifier, for each monotherapy pair, we calculated the Pearson correlation between expression of genes that are differentially expressed in either monotherapy (FDR < 0.1) in the NCI-DREAM data. We ranked the resulting correlations in descending order to calculate a ranking of drug synergy. To test performance by the same measures as the NCI-DREAM challenge, we used the PC-index as well as the AUROC and AUPR for synergistic drug combination. We used the code provided by the Challenge organizers to calculate the PC-index. For the AUC analysis, we used the same criteria as in the dream challenge for the definition of phenotypic synergy resulting in 16 synergistic drug pairs out of the total 91 pairs. To compare our method to DIGRE, we computed the Bayes factor (48), a bootstrapped performance distribution between two classifiers. A Bayes

factor of 2, for example, means that the first classifier outperformed the second at a 2-to-1 ratio. Two methods that have a Bayes factor < 3 may be considered statistically indistinguishable (49).

References

1. Al-Lazikani B, Banerji U, Workman P. Combinatorial drug therapy for cancer in the post-genomic era. Nat Biotechnol. 2012;30(7):679-92.
2. Ellegaard A-M, Dehlendorff C, Vind AC, Anand A, Cederkvist L, Petersen NHT, et al. Repurposing Cationic Amphiphilic Antihistamines for Cancer Treatment. EBioMedicine. 2016;9:130-9.
3. Palmer AC, Sorger PK. Combination Cancer Therapy Can Confer Benefit via Patient-to-Patient Variability without Drug Additivity or Synergy. Cell. 2017;171(7):1678-91.e13.
4. Gerlinger M, Rowan AJ, Horswell S, Math M, Larkin J, Endesfelder D, et al. Intratumor heterogeneity and branched evolution revealed by multiregion sequencing. N Engl J Med. 2012;366(10):883-92.
5. Hyman DM, Taylor BS, Baselga J. Implementing Genome-Driven Oncology. Cell. 2017;168(4):584-99.
6. Larkin J, Chiarion-Sileni V, Gonzalez R, Grob JJ, Cowey CL, Lao CD, et al. Combined Nivolumab and Ipilimumab or Monotherapy in Untreated Melanoma. N Engl J Med. 2015;373(1):23-34.
7. Baselga J, Bradbury I, Eidtmann H, Di Cosimo S, de Azambuja E, Aura C, et al. Lapatinib with trastuzumab for HER2-positive early breast cancer (NeoALTTO): a randomised, open-label, multicentre, phase 3 trial. Lancet. 2012;379(9816):633-40.
8. Greco WR, Faessel H, Levasseur L. The search for cytotoxic synergy between anticancer agents: a case of Dorothy and the ruby slippers? J Natl Cancer Inst. 1996;88(11):699-700.
9. LoRusso PM, Canetta R, Wagner JA, Balogh EP, Nass SJ, Boerner SA, et al. Accelerating Cancer Therapy Development: The Importance of Combination Strategies and Collaboration. Summary of an Institute of Medicine Workshop. Clin Cancer Res. 2012;18(22):6101-9.

10. Lehár J, Krueger AS, Avery W, Heilbut AM, Johansen LM, Price ER, et al. Synergistic drug combinations tend to improve therapeutically relevant selectivity. Nat Biotechnol. 2009;27(7):659-66.

11. Greco WR, Bravo G, Parsons JC. The search for synergy: a critical review from a response surface perspective. Pharmacol Rev. 1995;47(2):331-85.

12. Wolff AC, Lazar AA, Bondarenko I, Garin AM, Brincat S, Chow L, et al. Randomized Phase III Placebo-Controlled Trial of Letrozole Plus Oral Temsirolimus As First-Line Endocrine Therapy in Postmenopausal Women With Locally Advanced or Metastatic Breast Cancer. J Clin Oncol. 2013;31(2):195-202.

13. Bollenbach T, Quan S, Chait R, Kishony R. Nonoptimal microbial response to antibiotics underlies suppressive drug interactions. Cell. 2009;139(4):707-18.

14. Jiang P, Lee W, Li X, Johnson C, Liu JS, Brown M, et al. Genome-Scale Signatures of Gene Interaction from Compound Screens Predict Clinical Efficacy of Targeted Cancer Therapies. Cell Syst. 2018;6(3):343-54.e5.

15. Mott BT, Eastman RT, Guha R, Sherlach KS, Siriwardana A, Shinn P, et al. High-throughput matrix screening identifies synergistic and antagonistic antimalarial drug combinations. Sci Rep. 2015;5:13891.

16. Mathews Griner LA, Guha R, Shinn P, Young RM, Keller JM, Liu D, et al. High-throughput combinatorial screening identifies drugs that cooperate with ibrutinib to kill activated B-cell–like diffuse large B-cell lymphoma cells. Proceedings of the National Academy of Sciences. 2014;111(6):2349-54.

17. Borisy AA, Elliott PJ, Hurst NW, Lee MS, Lehar J, Price ER, et al. Systematic discovery of multicomponent therapeutics. Proc Natl Acad Sci U S A. 2003;100(13):7977-82.

18. Fitzgerald JB, Schoeberl B, Nielsen UB, Sorger PK. Systems biology and combination therapy in the quest for clinical efficacy. Nat Chemr Biol. 2006;2(9):458-66.

19. Bansal M, Yang J, Karan C, Menden MP, Costello JC, Tang H, et al. A community computational challenge to predict the activity of pairs of compounds. Nat Biotechnol. 2014;32(12):213-1222.

20. Saez-Rodriguez J, Costello JC, Friend SH, Kellen MR, Mangravite L, Meyer P, et al. Crowdsourcing biomedical research: leveraging communities as innovation engines. Nat Rev Genet. 2016;17(8):470-86.

21. Sun Y, Sheng Z, Ma C, Tang K, Zhu R, Wu Z, et al. Combining genomic and network characteristics for extended capability in predicting synergistic drugs for cancer. Nat Commun. 2015;6:8481.

22. Niepel M, Hafner M, Duan Q, Wang Z, Paull EO, Chung M, et al. Common and cell-type specific responses to anti-cancer drugs revealed by high throughput transcript profiling. Nat Commun. 2017;8(1):1186.

23. Yang J, Tang H, Li Y, Zhong R, Wang T, Wong S, et al. DIGRE: Drug-Induced Genomic Residual Effect Model for Successful Prediction of Multidrug Effects. CPT Pharmacometrics Syst Pharmacol. 2015;4(2):e1.

24. Goswami CP, Cheng L, Alexander PS, Singal A, Li L. A New Drug Combinatory Effect Prediction Algorithm on the Cancer Cell Based on Gene Expression and Dose-Response Curve. CPT Pharmacometrics Syst Pharmacol. 2015;4(2):e9.

25. Lee AV, Oesterreich S, Davidson NE. MCF-7 cells--changing the course of breast cancer research and care for 45 years. J Natl Cancer Inst. 2015;107(7).

26. Takahashi Y, Perkins SN, Hursting SD, Wang TTY. 17beta-Estradiol differentially regulates androgen-responsive genes through estrogen receptor-beta- and extracellular-signal regulated kinase-dependent pathways in LNCaP human prostate cancer cells. Mol Carcinog. 2007;46(2):117-29.

27. Early Breast Cancer Trialists' Collaborative G, Davies C, Godwin J, Gray R, Clarke M, Cutter D, et al. Relevance of breast cancer hormone receptors and other factors to the efficacy of adjuvant tamoxifen: patient-level meta-analysis of randomised trials. Lancet. 2011;378(9793):771-84.

28. Early Breast Cancer Trialists' Collaborative G. Aromatase inhibitors versus tamoxifen in early breast cancer: patient-level meta-analysis of the randomised trials. Lancet. 2015;386(10001):1341-52.

29. Haibe-Kains B, El-Hachem N, Birkbak NJ, Jin AC, Beck AH, Aerts HJWL, et al. Inconsistency in large pharmacogenomic studies. Nature. 2013;504(7480):389-93.

30. Ben-David U, Siranosian B, Ha G, Tang H, Oren Y, Hinohara K, et al. Genetic and transcriptional evolution alters cancer cell line drug response. Nature. 2018;560(7718):325-30.

31. Mattson MP, Calabrese EJ. Hormesis: what it is and why it matters. Hormesis: Springer; 2010. p. 1-13.

32. Li X, Yang T, Sun Z. Hormesis in Health and Chronic Diseases. Trends Endocrinol Metab. 2019;30(12):944-58.

33. Mattson MP. Hormesis and disease resistance: activation of cellular stress response pathways. Hum Exp Toxicol. 2008;27(2):155-62.

34. Riffkin CD, Chung R, Wall DM, Zalcberg JR, Cowman AF, Foley M, et al. Modulation of the function of human MDR1 P-glycoprotein by the antimalarial drug mefloquine. Biochem Pharmacol. 1996;52(10):1545-52.

35. Sas-Chen A, Avraham R, Yarden Y. A crossroad of microRNAs and immediate early genes (IEGs) encoding oncogenic transcription factors in breast cancer. J Mammary Gland Biol Neoplasia. 2012;17(1):3-14.

36. Tullai JW, Schaffer ME, Mullenbrock S, Sholder G, Kasif S, Cooper GM. Immediate-early and delayed primary response genes are distinct in function and genomic architecture. J Biol Chem. 2007;282(33):23981-95.

37. Chen EY, Tan CM, Kou Y, Duan Q, Wang Z, Meirelles GV, et al. Enrichr: interactive and collaborative HTML5 gene list enrichment analysis tool. BMC Bioinformatics. 2013;14:128.

38. Kuleshov MV, Jones MR, Rouillard AD, Fernandez NF, Duan Q, Wang Z, et al. Enrichr: a comprehensive gene set enrichment analysis web server 2016 update. Nucleic Acids Res. 2016;44(W1):W90-7.

39. Hanahan D, Weinberg RA. Hallmarks of cancer: the next generation. Cell. 2011;144(5):646-74.

40. Sirci F, Napolitano F, Pisonero-Vaquero S, Carrella D, Medina DL, di Bernardo D. Comparing structural and transcriptional drug networks reveals signatures of drug activity and toxicity in transcriptional responses. NPJ Syst Biol Appl. 2017;3:23.

41. Nioi P, Perry BK, Wang E-J, Gu Y-Z, Snyder RD. In vitro detection of drug-induced phospholipidosis using gene expression and fluorescent phospholipid based methodologies. Toxicol Sci. 2007;99(1):162-73.

42. Nadanaciva S, Lu S, Gebhard DF, Jessen BA, Pennie WD, Will Y. A high content screening assay for identifying lysosomotropic compounds. Toxicol In Vitro. 2011;25(3):715-23.

43. Woo JH, Shimoni Y, Yang WS, Subramaniam P, Iyer A, Nicoletti P, et al. Elucidating Compound Mechanism of Action by Network Perturbation Analysis. Cell. 2015;162(2):441-51.

44. Lefebvre C, Rajbhandari P, Alvarez MJ, Bandaru P, Lim WK, Sato M, et al. A human B-cell interactome identifies MYB and FOXM1 as master regulators of proliferation in germinal centers. Mol Syst Biol. 2010;6:377.

45. Alvarez MJ, Shen Y, Giorgi FM, Lachmann A, Ding BB, Ye BH, et al. Functional characterization of somatic mutations in cancer using network-based inference of protein activity. Nat Genet. 2016;48(8):838-47.

46. Pakos-Zebrucka K, Koryga I, Mnich K, Ljujic M, Samali A, Gorman AM. The integrated stress response. EMBO Rep. 2016:e201642195.

47. López-Maury L, Marguerat S, Bähler J. Tuning gene expression to changing environments: from rapid responses to evolutionary adaptation. Nat Rev Genet. 2008;9(8):583-93.

48. Bayes Factors. In: Balakrishnan N, Colton T, Everitt B, Piegorsch W, Ruggeri F, Teugels JL, editors. Wiley StatsRef: Statistics Reference Online. Lectures Notes of the Institute of Mathematical Statistics. 90. Chichester, UK: John Wiley & Sons, Ltd; 2014. p. 1-14.

49. Kass RE, Raftery AE. Bayes Factors. J Am Stat Assoc. 1995;90(430):773-95.

50. Shiau AK, Barstad D, Loria PM, Cheng L, Kushner PJ, Agard DA, et al. The structural basis of estrogen receptor/coactivator recognition and the antagonism of this interaction by tamoxifen. Cell. 1998;95(7):927-37.

51. Sharma N, Thomas S, Golden EB, Hofman FM, Chen TC, Petasis NA, et al. Inhibition of autophagy and induction of breast cancer cell death by mefloquine, an antimalarial agent. Cancer Lett. 2012;326(2):143-54.

52. Tang Z, Wu C, Wang T, Lao K, Wang Y, Liu L, et al. Design, synthesis and evaluation of 6-aryl-indenoisoquinolone derivatives dual targeting ERα and VEGFR-2 as anti-breast cancer agents. Eur J Med Chem. 2016;118:328-39.

53. Li X, Wu C, Lin X, Cai X, Liu L, Luo G, et al. Synthesis and biological evaluation of 3-aryl-quinolin derivatives as anti-breast cancer agents targeting ERα and VEGFR-2. Eur J Med Chem. 2019;161:445-55.

54. Tang Z, Niu S, Liu F, Lao K, Miao J, Ji J, et al. Synthesis and biological evaluation of 2,3-diaryl isoquinolinone derivatives as anti-breast cancer agents targeting ERα and VEGFR-2. Bioorg Med Chem Lett. 2014;24(9):2129-33.

55. Cook KL, Wärri A, Soto-Pantoja DR, Clarke PAG, Idalia Cruz M, Zwart A, et al. Chloroquine Inhibits Autophagy to Potentiate Antiestrogen Responsiveness in ER+ Breast Cancer. Clin Cancer Res. 2014;20(12):3222-32.

56. Rummukainen J, Kytölä S, Karhu R, Farnebo F, Larsson C, Isola JJ. Aberrations of chromosome 8 in 16 breast cancer cell lines by comparative genomic hybridization,

fluorescence in situ hybridization, and spectral karyotyping. Cancer Genet Cytogenet. 2001;126(1):1-7.

57. Shimada M, Imura J, Kozaki T, Fujimori T, Asakawa S, Shimizu N, et al. Detection of Her2/neu, c-MYC and ZNF217 gene amplification during breast cancer progression using fluorescence in situ hybridization. Oncol Rep. 2005;13(4):633-41.

58. Shadeo A, Lam WL. Comprehensive copy number profiles of breast cancer cell model genomes. Breast Cancer Res. 2006;8(1):R9.

59. Shajahan-Haq AN, Cook KL, Schwartz-Roberts JL, Eltayeb AE, Demas DM, Warri AM, et al. MYC regulates the unfolded protein response and glucose and glutamine uptake in endocrine resistant breast cancer. Mol Cancer. 2014;13:239.

60. Ellenrieder V. TGFbeta regulated gene expression by Smads and Sp1/KLF-like transcription factors in cancer. Anticancer Res. 2008;28(3A):1531-9.

61. Chen H, Tritton TR, Kenny N, Absher M, Chiu JF. Tamoxifen induces TGF-beta 1 activity and apoptosis of human MCF-7 breast cancer cells in vitro. J Cell Biochem. 1996;61(1):9-17.

62. Samaddar JS, Gaddy VT, Duplantier J, Thandavan SP, Shah M, Smith MJ, et al. A role for macroautophagy in protection against 4-hydroxytamoxifen-induced cell death and the development of antiestrogen resistance. Mol Cancer Ther. 2008;7(9):2977-87.

63. Klionsky DJ, Emr SD. Autophagy as a regulated pathway of cellular degradation. Science. 2000;290(5497):1717-21.

64. Shin JH, Bae D-J, Kim ES, Kim HB, Park SJ, Jo YK, et al. Autophagy Regulates Formation of Primary Cilia in Mefloquine-Treated Cells. Biomol Ther. 2015;23(4):327-32.

65. Shin JH, Park SJ, Jo YK, Kim ES, Kang H, Park J-H, et al. Suppression of autophagy exacerbates Mefloquine-mediated cell death. Neurosci Lett. 2012;515(2):162-7.

66. Wang X, Eno CO, Altman BJ, Zhu Y, Zhao G, Olberding KE, et al. ER stress modulates cellular metabolism. Biochem J. 2011;435(1):285-96.

67. Boya P, González-Polo R-A, Casares N, Perfettini J-L, Dessen P, Larochette N, et al. Inhibition of macroautophagy triggers apoptosis. Mol Cell Biol. 2005;25(3):1025-40.

68. Faust PL, Kovacs WJ. Cholesterol biosynthesis and ER stress in peroxisome deficiency. Biochimie. 2014;98:75-85.

69. Christian P, Su Q. MicroRNA regulation of mitochondrial and ER stress signaling pathways: implications for lipoprotein metabolism in metabolic syndrome. Am J Physiol Endocrinol Metab. 2014;307(9):E729-37.

70. Meyer SN, Amoyel M, Bergantiños C, de la Cova C, Schertel C, Basler K, et al. An ancient defense system eliminates unfit cells from developing tissues during cell competition. Science. 2014;346(6214):1258236.

71. Schaefer L. Complexity of danger: the diverse nature of damage-associated molecular patterns. J Biol Chem. 2014;289(51):35237-45.

72. Pandey S, Singh S, Anang V, Bhatt AN, Natarajan K, Dwarakanath BS. Pattern Recognition Receptors in Cancer Progression and Metastasis. Cancer Growth Metastasis. 2015;8:25-34.

73. Muralidharan S, Mandrekar P. Cellular stress response and innate immune signaling: integrating pathways in host defense and inflammation. J Leukoc Biol. 2013;94(6):1167-84.

74. Chen X, Houten S, Allette K, Sebra RP, Stolovitzky G, Losic B. Characterization of drug-induced splicing complexity in prostate cancer cell line using long read technology. Biocomputing 2018: WORLD SCIENTIFIC; 2017. p. 8-19.

75. Pan Q, Shai O, Misquitta C, Zhang W, Saltzman AL, Mohammad N, et al. Revealing global regulatory features of mammalian alternative splicing using a quantitative microarray platform. Mol Cell. 2004;16(6):929-41.

76. Holbeck SL, Camalier R, Crowell JA, Govindharajulu JP, Hollingshead M, Anderson LW, et al. The National Cancer Institute ALMANAC: A Comprehensive Screening Resource for the Detection of Anticancer Drug Pairs with Enhanced Therapeutic Activity. Cancer Res. 2017;77(13):3564-76.

77. Held MA, Langdon CG, Platt JT, Graham-Steed T, Liu Z, Chakraborty A, et al. Genotype-selective combination therapies for melanoma identified by high-throughput drug screening. Cancer Discov. 2013;3(1):52-67.

78. Bliss CI. The Toxicity of poisons applied jointly. Ann Appl Biol. 1939;26(3):585-615.

79. Chou T-C, Talalay P. Quantitative analysis of dose-effect relationships: the combined effects of multiple drugs or enzyme inhibitors. Adv Enzyme Regul. 1984;22:27-55.

80. Chou TC, Martin N. CompuSyn for drug combinations: PC software and user's guide: a computer program for quantitation of synergism and antagonism in drug combinations, and the determination of IC50 and ED50 and LD50 values. ComboSyn, Paramus, NJ. 2005.

81. Dobin A, Davis CA, Schlesinger F, Drenkow J, Zaleski C, Jha S, et al. STAR: ultrafast universal RNA-seq aligner. Bioinformatics. 2013;29(1):15-21.

82. Liao Y, Smyth GK, Shi W. featureCounts: an efficient general purpose program for assigning sequence reads to genomic features. Bioinformatics. 2014;30(7):923-30.

83. Robinson MD, Oshlack A. A scaling normalization method for differential expression analysis of RNA-seq data. Genome Biol. 2010;11(3):R25.
84. Law CW, Chen Y, Shi W, Smyth GK. voom: Precision weights unlock linear model analysis tools for RNA-seq read counts. Genome Biol. 2014;15(2):R29.
85. Ritchie ME, Phipson B, Wu D, Hu Y, Law CW, Shi W, et al. limma powers differential expression analyses for RNA-sequencing and microarray studies. Nucleic Acids Res. 2015;43(7):e47.
86. Benjamini Y, Hochberg Y. Controlling the False Discovery Rate: A Practical and Powerful Approach to Multiple Testing. J R Stat Soc Series B Stat Methodol. 1995;57(1):298-300.
87. Hartigan JA, Wong MA. Algorithm AS 136: A K-Means Clustering Algorithm. Appl Stat. 1979;28(1):100.
88. Jones E, Oliphant T, Paterson P, others. SciPy: Open source scientific tools for Python. 2001.
89. Liberzon A, Subramanian A, Pinchback R, Thorvaldsdottir H, Tamayo P, Mesirov JP. Molecular signatures database (MSigDB) 3.0. Bioinformatics. 2011;27(12):1739-40.
90. Subramanian A, Tamayo P, Mootha VK, Mukherjee S, Ebert BL, Gillette MA, et al. Gene set enrichment analysis: A knowledge-based approach for interpreting genome-wide expression profiles. Proceedings of the National Academy of Sciences. 2005;102(43):15545-50.
91. Bhat-Nakshatri P, Wang G, Collins NR, Thomson MJ, Geistlinger TR, Carroll JS, et al. Estradiol-regulated microRNAs control estradiol response in breast cancer cells. Nucleic Acids Res. 2009;37(14):4850-61.
92. Seabold S, Perktold J. Statsmodels: Econometric and statistical modeling with python. Proceedings of the 9th Python in Science Conference.
93. Ashburner M, Ball CA, Blake JA, Botstein D, Butler H, Cherry JM, et al. Gene ontology: tool for the unification of biology. The Gene Ontology Consortium. Nat Genet. 2000;25(1):25-9.
94. Hu Y, Huang Y, Du Y, Orellana CF, Singh D, Johnson AR, et al. DiffSplice: the genome-wide detection of differential splicing events with RNA-seq. Nucleic Acids Res. 2013;41(2):e39.
95. Simes RJ. An Improved Bonferroni Procedure for Multiple Tests of Significance. Biometrika. 1986;73(3):751.
96. Margolin AA, Nemenman I, Basso K, Wiggins C, Stolovitzky G, Dalla Favera R, et al. ARACNE: an algorithm for the reconstruction of gene regulatory networks in a mammalian cellular context. BMC Bioinformatics. 2006;7 Suppl 1:S7.

97. Lamb J. The Connectivity Map: a new tool for biomedical research. Nat Rev Cancer. 2007;7(1):54-60.

98. Li Q, Birkbak NJ, Gyorffy B, Szallasi Z, Eklund AC. Jetset: selecting the optimal microarray probe set to represent a gene. BMC Bioinformatics. 2011;12(1):474.

99. Foulkes NS, Sassone-Corsi P. More is better: activators and repressors from the same gene. Cell. 1992;68(3):411-4.

100. Wray GA. The Evolution of Transcriptional Regulation in Eukaryotes. Mol Biol Evol. 2003;20(9):1377-419.

101. Partridge CG, MacManes MD, Knapp R, Neff BD. Brain Transcriptional Profiles of Male Alternative Reproductive Tactics and Females in Bluegill Sunfish. PLoS One. 2016;11(12):e0167509.

Figure Legends

Figure 1: The Transcriptomics of Drug Combinations Mirror their Phenotypic Characteristics

A) Monotherapies and drug combinations used in the study. B) Workflow of molecular analysis of synergy. Starburst highlights the novel component of RNAseq analysis. Question mark denotes the focus of the study. C-H) Fold change over control of cell count for MCF7 cells (C-E) and LNCaP cells (F-H) treated with Tamoxifen and Mefloquine (C,F), Mefloquine and Withaferin (D,G), and Tamoxifen and Withaferin (E,H). Dashed line indicates predicted viability of the combination based on the Bliss model. Excess Over Bliss (EOB) ± $Error_{EOB}$ is given for the 12, 24, and 48 hr time points (see Methods). I) Average gene expression for each treatment and time point in the MCF7 combination experiments (covering 108 treatment and 18 DMSO samples). G) Principal component analysis of gene expression for the average over replicates at each treatment and time point in the MCF7 combination and dose experiments. (See also Supplementary Files 3-9, and Source Data File 1.)

Figure 1-figure supplement 1: The response of MCF7 to TM is more synergistic than to TW

A) Combination Index for the combinations at the selected doses. Combination Index < 1 indicates synergy. B) Viability of MCF7 cells treated with increasing doses of T and M performed alongside RNA collection at 24 hours, compared to TM (Figure 1). (See also Supplementary Files 1-2.)

Figure 1-figure supplement 2: Transcriptomic profiles of MFC7 and LNCaP cells with combinations

A) Similarity between the gene expression data of two replicates treated with TM at 12 hours. B) The gene expression of one replicate treated with TM at 12 hours and another replicate treated

with TM at 3 hours shows differential expression beyond the replicates of (A). C) Average gene expression for each treatment and time point in the LNCaP combination experiments (covering 108 treatment and 18 DMSO samples). D) Average gene expression for each treatment and time point in the MCF7 dose experiments. E) Principal component analysis of gene expression for the average over replicates at each treatment and time point in the MCF7 combination and dose experiments. (See also Source Data Files 2-3.)

Figure 2: Synergistically expressed genes and correlated monotherapies are associated with synergy A-C) Number of DEGs over time in MCF7. The Venn diagrams correspond to DEGs at 3 hours in A) T, M, and TM, B) T, W, and TW, and C) M, W, and MW. The area represented in each color is in proportion to the number of genes in the corresponding color of the Venn diagram; blue areas represent SEGs. D-E) Relationship of Excess Over Bliss score with D) the number of SEGs, and E) correlation in gene expression values between each pair of monotherapies. Note that some of the "pairs" from the dose experiments represent the same dataset correlation with itself (i.e. T 10 μM with T 10 μM for the T 20 μM "combination") and so have correlation = 1.0 as expected, and are shown for clarity. (See also Source Data Files 4-6.)

Figure 2-figure supplement 1: Gene expression characteristics of differential expression and synergy in MCF7 A) Comparison between gene expression in treatment (y-axis) and control (x-axis), for all genes over all treatments from the combination experiments in MCF7. Upregulated and downregulated genes as determined by Limma with Voom are in red and blue respectively corresponding to a FDR < 1E-18, and green lines represent fold change over control of 2. B) Choice of FDR cutoff for the dose experiments. The FDR cutoff is represented as *1E-n*, with *n* denoted next to each point. C-D). Percentage of differentially expressed genes that are synergistic in each combination according to FDR corrected p-value at C) 3 hours and D) 12 hours in MCF7 cells. (See also Source Data Files 4-5.)

Figure 2-figure supplement 2: Differential expression in LNCaP Number of DEGs over time in LNCaP. The Venn diagrams correspond to DEGs at 3 hours in A) T, M, and TM, B) T, W, and TW, and C) M, W, and MW. The area represented in each color is in proportion to the number of genes in the corresponding color of the Venn diagram; blue areas represent SEGs. (See also Source Data File 6.)

Figure 3: Key biological processes are associated with synergy Enrichment of DEGs in T, M, and TM with cancer-relevant gene sets. Only gene sets enriched in at least one condition (time point or treatment) are shown. "T∪M" indicates the union of DEGs after in T or M. Color intensity reflects degree of enrichment by Fisher's Exact test. Color markers indicate treatment and color marker intensity indicates dose. * = hallmark of cancer, † = drug target (see Methods).

Figure 3-figure supplement 1: Biological processes in MCF7 and LNCaP A) Enrichment scores of differentially up and down regulated genes at different time points in W, M, T, TW, and MW, in MCF7 cells with the same cancer-relevant gene sets shown in figure 3. B) Hierarchical clustering of enrichment scores of differentially up and down regulated genes at different time

points in the combination experiments in LNCaP cells with significant biological process gene sets (see Methods). "U" indicates the union of two genes sets, and represents the expected differentially expressed genes if the interaction between drugs was additive. Color intensity reflects the degree of enrichment by Fisher's Exact test and is shown as $-\log_{10}$(FDR corrected p-value). Red: M, Blue: T, Yellow: W, Orange: MW, Green: TW, Magenta: TM.

Figure 3-figure supplement 2: Cellular components are synergistic in TM but not in withaferin combinations in LNCaP Enrichment of DEGs with cellular component gene sets (see Methods) in A) MCF7 cells for T, M, and TM, B) MCF7 cells for W, M, T, TW, and MW, and C) all treatments in LNCaP cells, shown with hierarchical clustering (see Methods). Only gene sets enriched in at least one condition (time point or treatment) are shown. For gene sets that also appeared in the top 40 gene sets associated with phospholipidosis (Supplementary Table 6 of Sirci et al.), the rank of the gene set in that list is shown in parentheses. "U" indicates the union of two genes sets, and represents the expected differentially expressed genes if the interaction between drugs was additive. Color intensity reflects the degree of enrichment by Fisher's Exact test and is shown as $-\log_{10}$(FDR corrected p-value). In A and C, the two PLD genes sets are also shown on a larger color scale (see inset colorbar) to illustrate subtle differences in enrichment. Red: M, Blue: T, Yellow: W, Orange: MW, Green: TW, Magenta: TM.

Figure 4: Differentially expressed genes have different time courses A) Mean and standard deviation of gene expression in four clusters identified according to their similarity in expression in T, M, and TM. B) Examples of genes in each cluster with significantly different trajectories in TM than the monotherapies. C) Enrichment of the same biological processes as in Figure 2F in the clusters. (See also Source Data File 7.)

Figure 5: New differential splicing emerges in drug combination TM Top 100 synergistically spliced exons in combination TM at 12 hours.

Figure 6: Synergistic splicing is distinct from differential expression and associated with synergy A) Number of synergistically expressed and synergistically spliced genes in TM over time; shaded areas correspond to the Venn diagram for 3 hours. B) Relationship of Excess Over Bliss score with the number of synergistically spliced genes. (See also Supplementary File 9.)

Figure 6-figure supplement 1: Differential and synergistic splicing A-C) Number of differentially spliced genes over time with Venn diagrams of differentially spliced genes at 3 hours in a) T, M, and TM, b) T, W, and TW, and c) M, W, and MW. The area represented in each color is in proportion to the number of genes in the corresponding color of the Venn diagram; blue areas represent synergistic genes. d-f) Number of synergistically expressed and synergistically spliced genes in d) TM, e) TW, and f) MW over time; shaded areas correspond to the Venn diagrams for 3 hours. (See also Source Data File 8.)

Figure 7: New differentially active transcription factors emerge in combination TM Number of DATFs over time with Venn diagrams at 3 hours in A) T, M, and TM, B) T, W, and

TW, and C) M, W, and MW. Area represented in each color matches the number of genes in the corresponding color of the Venn diagram; blue areas represent synergistic TFs. (See also Source Data File 9.)

Figure 7-figure supplement 1: Possible changes to transcription factor activity Four cases of transcription factor activity that were assessed to determine whether a transcription factor was activated or inactivated.

Figure 7-figure supplement 2: Classes of differentially active transcription factors A) Differentially active transcription factors for each combination according to the status of the positive and negative effector of each transcription factor. Unique: either positive or negative effector, but not both, is differentially active; concordant: both effectors are activated or both are inactivated; discordant: one effector is activated and the other is inactivated. B) Differentially active transcription factors for each combination according to each of the four cases supplement 1.

Figure 8: Characteristics of differentially active transcription factors A) All instances of DATFs according to the differential expression or splicing status of each TF in the corresponding treatment and time point. The top 20 most significant DATFs not differentially expressed nor spliced are listed. All 20 are positive effectors. Arrows: up = activated, down = inactivated. B) Heatmap of DATFs over time in T, M, and TM at 3-24 hours. Color intensity reflects the degree and direction of enrichment by Fisher's Exact test with red for activation and blue for inactivation. Only significant instances are shown. C) Enrichment of gene clusters from Figure 2F with sets of TF targets. Color intensity reflects the degree of enrichment by Fisher's Exact test. (See also Source Data File 9.)

Figure 8-figure supplement 1: Differentially active transcription factors in W combinations Heatmap of differentially active transcription factors over time in Withaferin, MW, and TW at 3-24 hours. Color intensity reflects the degree and direction of enrichment by Fisher's Exact test and is shown as $-\log_{10}$(FDR corrected p-value), with positive values for activation and negative values for inactivation.

Figure 9: Transcription factors become differentially active in a time-dependent cascade in TM The number of DATFs or SEGs at 3-24 hours are shown as bubbles. Blue, red, and white bubbles represent DATFs in T, M, and TM, respectively. TFs (gray bubbles) and SEGs (green bubbles) shown are "explained" by the following mechanisms: double-down mechanism at the same (magenta arrow and number) or previous (angled magenta arrow) time point, the AND mechanism at the same (converging blue and red arrows and purple number) or previous (angled converging blue and red arrows) time point, or by connection to another TF "explained" by one of these mechanisms at the same (see supplement 1), or previous (vertical arrows) time point. The total number and percentage of TFs or SEGs in TM meeting any of these criteria is shown. (See also Source Data File 10.)

Figure 9-figure supplement 1: Cascade of differential transcription factor activity Connections between differentially active transcription factors in TM based on the MCF7 network. Each bubble represents a set of transcription factors that are differentially active in TM at a given timepoint. The codes on each bubble represent their differential activity status in Tamoxifen (first digit), Mefloquine, (second digit), and TM (third digit), where 1 is differentially active and 0 is not. Synergistic transcription factors in TM (001), are categorized into "explained" bubbles (gray) or not explained (white). At each timepoint, synergistic transcription factors can be "explained" by a network connection to a transcription factor that is differentially active in Tamoxifen and Mefloquine (111, magenta), or to at least one transcription factor in each of Tamoxifen alone (101, blue) and Mefloquine alone (011, red), or both, resulting in the left-hand, right-hand, and middle gray bubbles, respectively, in the middle layer. The fourth gray bubble in the lowest layer represents transcription factors which have connections to transcription factors in the middle "explained" layer, but not to transcription factors in the top layer. Numbers in italics represent synergistic transcription factors that can be explained by connections to transcription factors that were active in monotherapies at the previous time point (blue, magenta, and red bubbled with dashed outlines at top of each timepoint). At the right in each time point, the dashed-outline bubble represents "explained" transcription factors in the gray bubbles at the previous time point. Synergistic transcription factors not explained by other means which have a connection to any "explained" transcription factors at the previous time point are shown in the gray bubble below the dashed-outline bubble. Finally, synergistic transcription factors that cannot be explained by any network connections are shown in the white bubble resulting from the "null" set at each timepoint. The colors in this figure correspond to figure 9, and the sum of all gray bubbles at each timepoint in this figure correspond to the single gray bubble shown at each timepoint in figure 9. (See also Source Data File 10.)

Figure 10: Correlation of Monotherapies is Associated with Synergy in an Independent Dataset A) Relationship between Excess Over Bliss (EOB) for 91 drug pairs and the correlation between the gene expression of LY3 DLBCL cells treated with corresponding monotherapies in the DREAM dataset. The inset indicates the distribution of correlations for pairs with EOB < -2.5 and EOB > 2.5. B) Hypothetical model for the relationships between monotherapy correlation, SEGs, and synergy. Boxed nodes represent phenomena we directly measured in this study. C-D) ROC (C) and PR (D) for classification of synergistic drug pairs using expression correlation and DIGRE.

Table

T_0		TM_0		M_0		TW_0		MW_0		W_0	
FOS	-6	BCAN	-17	ATXN2	-3	**EGR1**	**-54**	**EGR1**	**-53**	**EGR1**	**-53**
MYC	-3	FOS	-17	JUN	-2	**JUN**	**-26**	**JUN**	**-28**	**IER2**	**-20**
TOB1	-3	VIM	-17	ZNF592	-1	**IER2**	**-23**	IER2	-17	**JUN**	**-19**

KLF4	-2	ETS1	-15	ZHX2	-1	JUNB	-17	PDCD7	-17	C17O	-16
SGK1	-2	MSN	-13	SCAF4	-1	PDCD7	-16	ZFP36	-15	ZFP36	-16
PRDM1	-2	NCAN	-10	NAT8L	-1	C17ORF91	-16	JUNB	-14	PDCD7	-15

Table: Selection of adjusted p-value cutoff for differentially expressed genes. The six most differentially expressed genes with respect to DMSO in each treatment at 0+ hours are shown in ascending order of their Voom score ($\log_{10}$(FDR)). Immediate Early Genes are marked in red. Differentially expressed genes according to the $1.0\ x10^{-18}$ cutoff for FDR corrected p-value are marked in bold.

Supplementary Files

Supplementary File 1: Viability data and calculated EOB for TM dose matrices at 12, 24, and 48 hours in MCF7. Actual values of negative inhibition in monotherapies are included in the heatmap at left. Monotherapy inhibition values used to calculate EOB are shown in the table at right (i.e. Drug1_NPI).

Supplementary File 2: Viability data and calculated EOB for TW dose matrices at 12, 24, and 48 hours in MCF7. Actual values of negative inhibition in monotherapies are included in the heatmap at left. Monotherapy inhibition values used to calculate EOB are shown in the table at right (i.e. Drug1_NPI).

Supplementary File 3: Time courses viability data of TM, TW, and MW in MCF7.

Supplementary File 4: Time courses viability data of TM, TW, and MW in LNCaP.

Supplementary File 5: Viability data and calculated EOB for TM, TW, and MW at 48 hours in LNCaP.

Supplementary File 6: Viability data for T and M dose and and calculated EOB for sham combinations in MCF7.

Supplementary File 7: Archive of Raw Fastq IDs

Supplementary File 8: Archive of Raw Expression Files

Supplementary File 9: Exon Counts

Source Data Files

Source Data File 1: Log counts per million of MCF7 cell combination treatment experiments

Source Data File 2: Log counts per million of MCF7 cell monotherapy dose experiments

Source Data File 3: Log counts per million of LNCaP cell combination treatment experiments

Source Data File 4: Archive of MCF7 combination experiments differential expression data

Source Data File 5: Archive of MCF7 dose experiments differential expression data

Source Data File 6: Archive of LNCaP differential expression data

Source Data File 7: k-means clusters assigned to genes

Source Data File 8: Archive of differential splicing data

Source Data File 9: Archive of differential transcription factor activity data

Source Data File 10: Archive of transcription factors involved in the transcriptional cascade

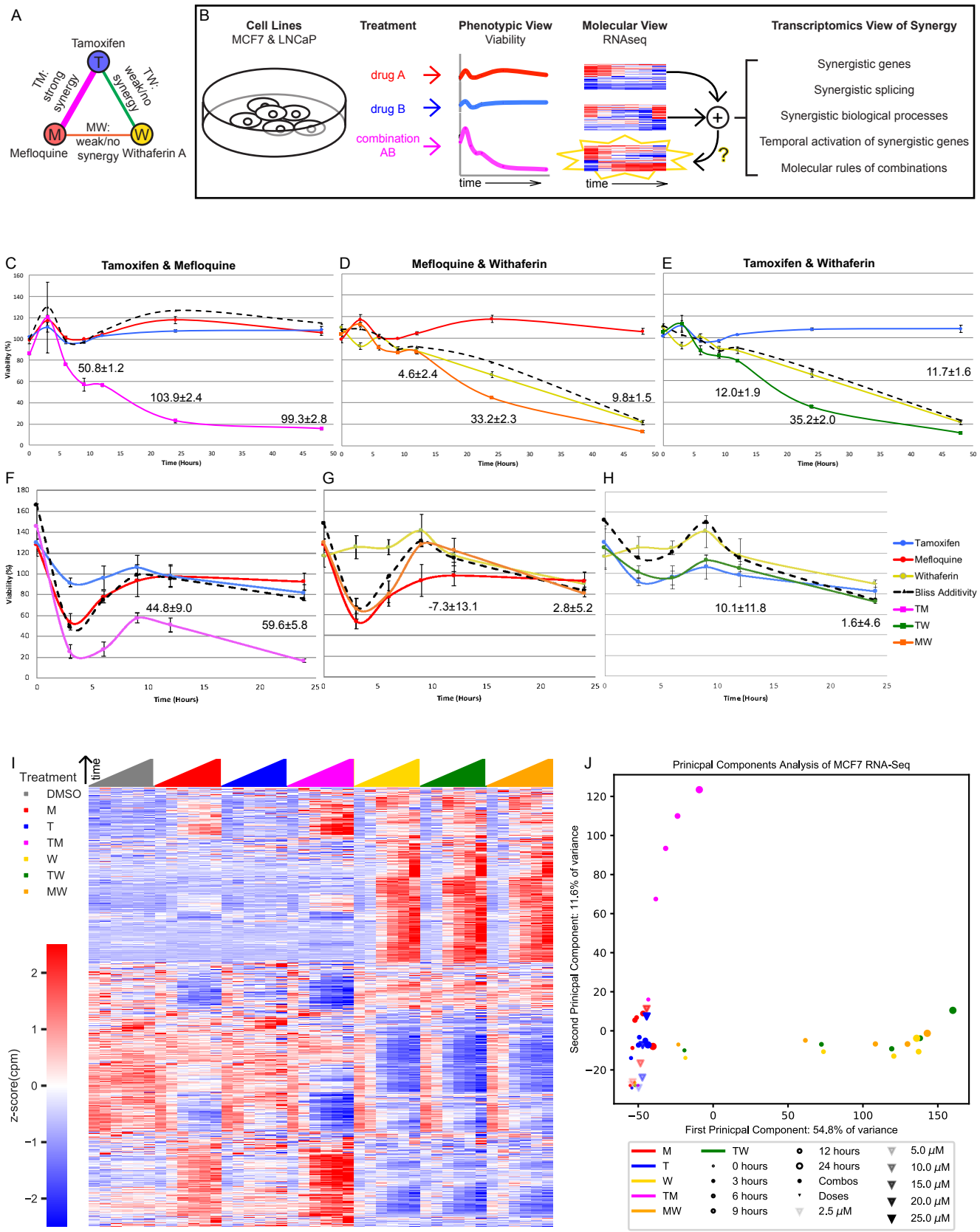
A
Tamoxifen
TM: strong synergy
TW: weak/no synergy
MW: weak/no synergy
Mefloquine
Withaferin A
B
Cell Lines
MCF7 & LNCaP
Treatment
drug A
drug B
combination AB
Phenotypic View
Viability
time
Molecular View
RNAseq
time
Transcriptomics View of Synergy
Synergistic genes
Synergistic splicing
Synergistic biological processes
Temporal activation of synergistic genes
Molecular rules of combinations
C
Tamoxifen & Mefloquine
50.8±1.2
103.9±2.4
99.3±2.8
Viability (%)
Time (Hours)
D
Mefloquine & Withaferin
4.6±2.4
9.8±1.5
33.2±2.3
Time (Hours)
E
Tamoxifen & Withaferin
11.7±1.6
12.0±1.9
35.2±2.0
Time (Hours)
F
44.8±9.0
59.6±5.8
Viability (%)
Time (Hours)
G
-7.3±13.1
2.8±5.2
Time (Hours)
H
10.1±11.8
1.6±4.6
Time (Hours)
Tamoxifen
Mefloquine
Withaferin
Bliss Additivity
TM
TW
MW
I
Treatment
time
DMSO
M
T
TM
W
TW
MW
z-score(cpm)
J
Prinicpal Components Analysis of MCF7 RNA-Seq
Second Prinicpal Component: 11.6% of variance
First Prinicpal Component: 54.8% of variance
M
T
W
TM
MW
TW
0 hours
3 hours
6 hours
9 hours
12 hours
24 hours
Combos
Doses
2.5 μM
5.0 μM
10.0 μM
15.0 μM
20.0 μM
25.0 μM

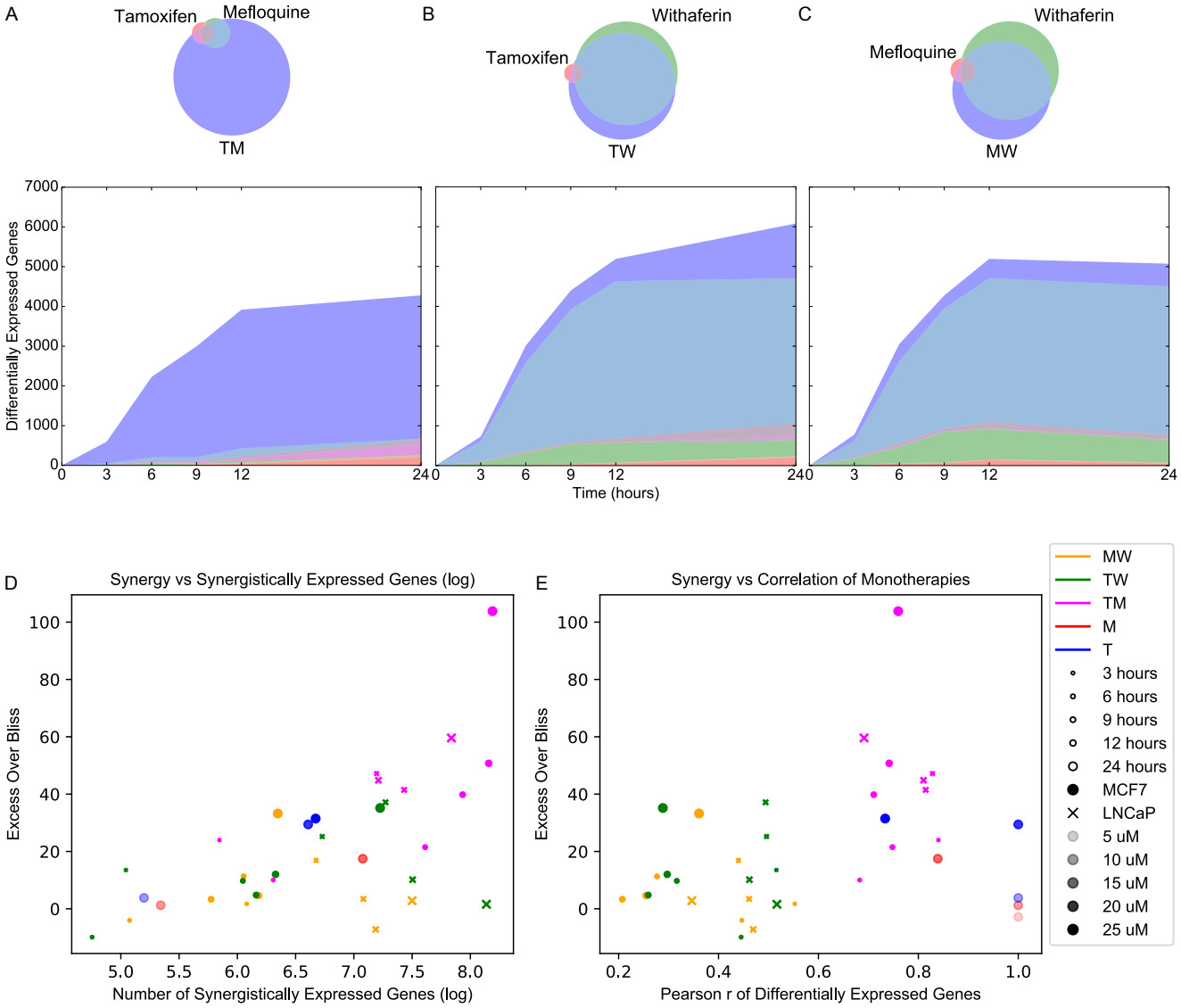
A
Tamoxifen
Mefloquine
TM
B
Tamoxifen
Withaferin
TW
C
Mefloquine
Withaferin
MW
Differentially Expressed Genes
Time (hours)
D
Synergy vs Synergistically Expressed Genes (log)
Excess Over Bliss
Number of Synergistically Expressed Genes (log)
E
Synergy vs Correlation of Monotherapies
Excess Over Bliss
Pearson r of Differentially Expressed Genes
MW
TW
TM
M
T
3 hours
6 hours
9 hours
12 hours
24 hours
MCF7
LNCaP
5 uM
10 uM
15 uM
20 uM
25 uM

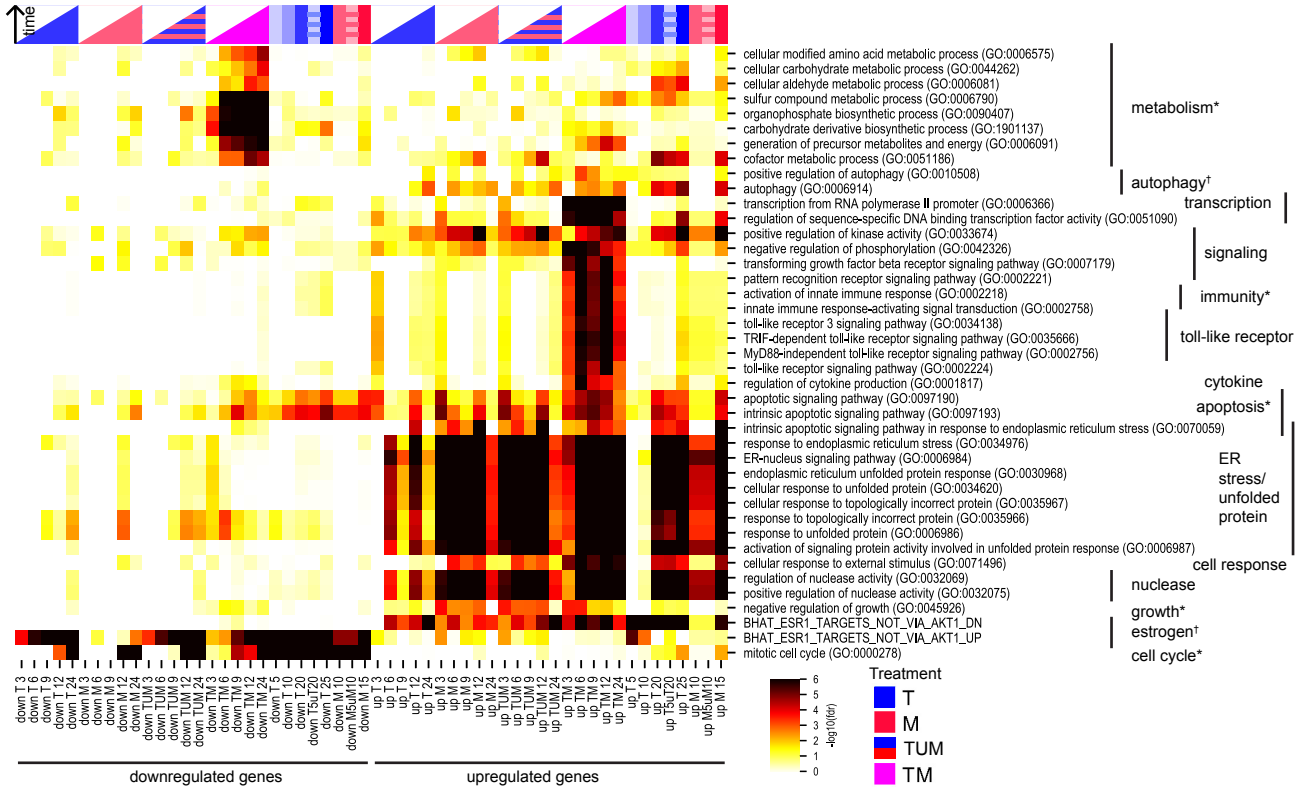
time
cellular modified amino acid metabolic process (GO:0006575)
cellular carbohydrate metabolic process (GO:0044262)
cellular aldehyde metabolic process (GO:0006081)
sulfur compound metabolic process (GO:0006790)
organophosphate biosynthetic process (GO:0090407)
carbohydrate derivative biosynthetic process (GO:1901137)
generation of precursor metabolites and energy (GO:0006091)
cofactor metabolic process (GO:0051186)
positive regulation of autophagy (GO:0010508)
autophagy (GO:0006914)
transcription from RNA polymerase II promoter (GO:0006366)
regulation of sequence-specific DNA binding transcription factor activity (GO:0051090)
positive regulation of kinase activity (GO:0033674)
negative regulation of phosphorylation (GO:0042326)
transforming growth factor beta receptor signaling pathway (GO:0007179)
pattern recognition receptor signaling pathway (GO:0002221)
activation of innate immune response (GO:0002218)
innate immune response-activating signal transduction (GO:0002758)
toll-like receptor 3 signaling pathway (GO:0034138)
TRIF-dependent toll-like receptor signaling pathway (GO:0035666)
MyD88-independent toll-like receptor signaling pathway (GO:0002756)
toll-like receptor signaling pathway (GO:0002224)
regulation of cytokine production (GO:0001817)
apoptotic signaling pathway (GO:0097190)
intrinsic apoptotic signaling pathway (GO:0097193)
intrinsic apoptotic signaling pathway in response to endoplasmic reticulum stress (GO:0070059)
response to endoplasmic reticulum stress (GO:0034976)
ER-nucleus signaling pathway (GO:0006984)
endoplasmic reticulum unfolded protein response (GO:0030968)
cellular response to unfolded protein (GO:0034620)
cellular response to topologically incorrect protein (GO:0035967)
response to topologically incorrect protein (GO:0035966)
response to unfolded protein (GO:0006986)
activation of signaling protein activity involved in unfolded protein response (GO:0006987)
cellular response to external stimulus (GO:0071496)
regulation of nuclease activity (GO:0032069)
positive regulation of nuclease activity (GO:0032075)
negative regulation of growth (GO:0045926)
BHAT_ESR1_TARGETS_NOT_VIA_AKT1_DN
BHAT_ESR1_TARGETS_NOT_VIA_AKT1_UP
mitotic cell cycle (GO:0000278)
metabolism*
autophagy†
transcription
signaling
immunity*
toll-like receptor
cytokine
apoptosis*
ER stress/ unfolded protein
cell response
nuclease
growth*
estrogen†
cell cycle*
down T 3
down T 6
down T 9
down T 12
down T 24
down M 3
down M 6
down M 9
down M 12
down M 24
down TUM 3
down TUM 6
down TUM 9
down TUM 12
down TUM 24
down TM 3
down TM 6
down TM 9
down TM 12
down TM 24
down T 5
down T 10
down T 20
down T5uT20
down T 25
down M 10
down M5uM10
down M 15
up T 3
up T 6
up T 9
up T 12
up T 24
up M 3
up M 6
up M 9
up M 12
up M 24
up TUM 3
up TUM 6
up TUM 9
up TUM 12
up TUM 24
up TM 3
up TM 6
up TM 9
up TM 12
up TM 24
up T 5
up T 10
up T 20
up T5uT20
up T 25
up M 10
up M5uM10
up M 15
downregulated genes
upregulated genes
-log10(fdr)
6
5
4
3
2
1
0
Treatment
T
M
TUM
TM

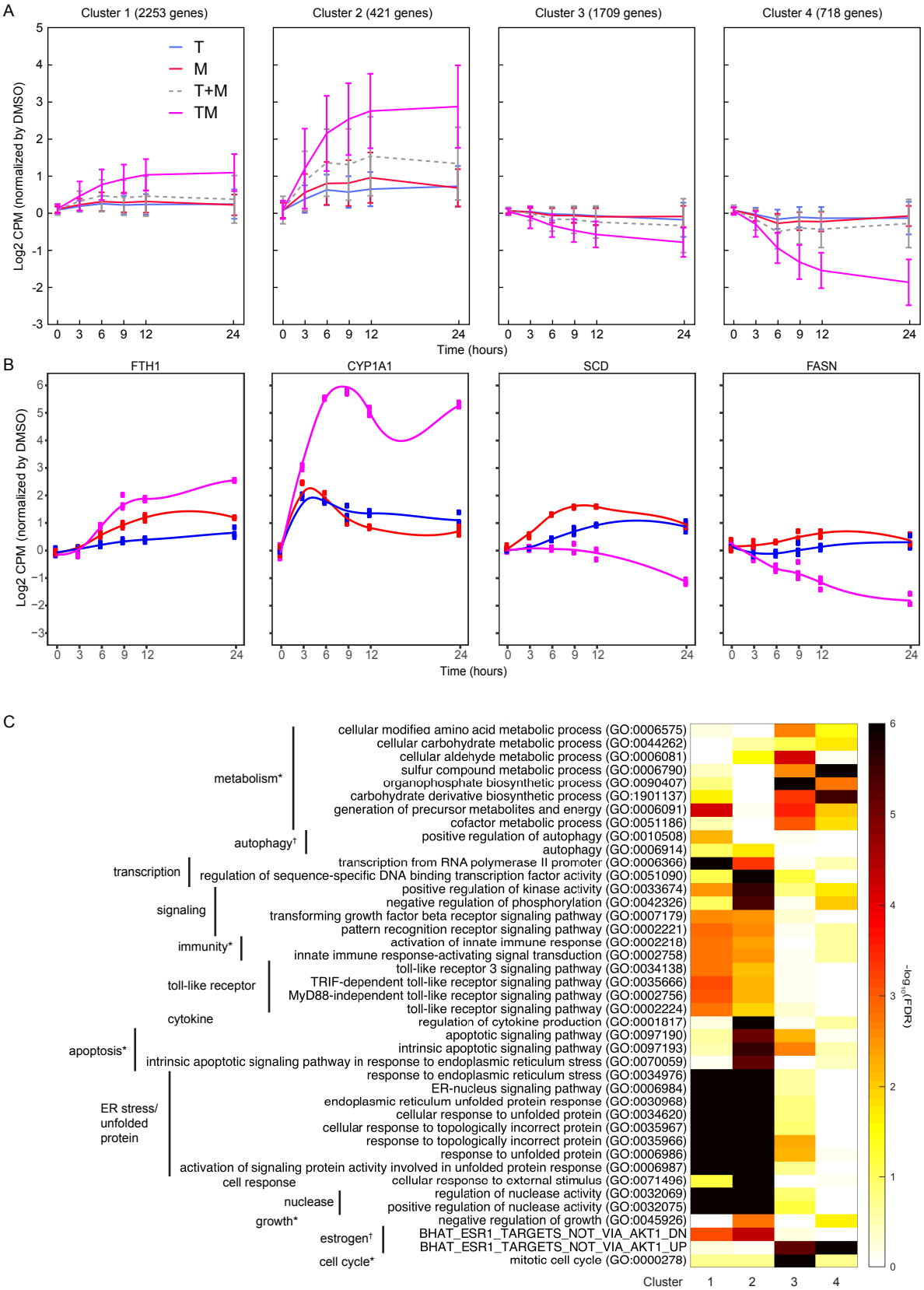
A
Cluster 1 (2253 genes)
Cluster 2 (421 genes)
Cluster 3 (1709 genes)
Cluster 4 (718 genes)
T
M
T+M
TM
Log2 CPM (normalized by DMSO)
Time (hours)
B
FTH1
CYP1A1
SCD
FASN
Log2 CPM (normalized by DMSO)
Time (hours)
C
metabolism*
autophagy†
transcription
signaling
immunity*
toll-like receptor
cytokine
apoptosis*
ER stress/ unfolded protein
cell response
nuclease
growth*
estrogen†
cell cycle*
cellular modified amino acid metabolic process (GO:0006575)
cellular carbohydrate metabolic process (GO:0044262)
cellular aldehyde metabolic process (GO:0006081)
sulfur compound metabolic process (GO:0006790)
organophosphate biosynthetic process (GO:0090407)
carbohydrate derivative biosynthetic process (GO:1901137)
generation of precursor metabolites and energy (GO:0006091)
cofactor metabolic process (GO:0051186)
positive regulation of autophagy (GO:0010508)
autophagy (GO:0006914)
transcription from RNA polymerase II promoter (GO:0006366)
regulation of sequence-specific DNA binding transcription factor activity (GO:0051090)
positive regulation of kinase activity (GO:0033674)
negative regulation of phosphorylation (GO:0042326)
transforming growth factor beta receptor signaling pathway (GO:0007179)
pattern recognition receptor signaling pathway (GO:0002221)
activation of innate immune response (GO:0002218)
innate immune response-activating signal transduction (GO:0002758)
toll-like receptor 3 signaling pathway (GO:0034138)
TRIF-dependent toll-like receptor signaling pathway (GO:0035666)
MyD88-independent toll-like receptor signaling pathway (GO:0002756)
toll-like receptor signaling pathway (GO:0002224)
regulation of cytokine production (GO:0001817)
apoptotic signaling pathway (GO:0097190)
intrinsic apoptotic signaling pathway (GO:0097193)
intrinsic apoptotic signaling pathway in response to endoplasmic reticulum stress (GO:0070059)
response to endoplasmic reticulum stress (GO:0034976)
ER-nucleus signaling pathway (GO:0006984)
endoplasmic reticulum unfolded protein response (GO:0030968)
cellular response to unfolded protein (GO:0034620)
cellular response to topologically incorrect protein (GO:0035967)
response to topologically incorrect protein (GO:0035966)
response to unfolded protein (GO:0006986)
activation of signaling protein activity involved in unfolded protein response (GO:0006987)
cellular response to external stimulus (GO:0071496)
regulation of nuclease activity (GO:0032069)
positive regulation of nuclease activity (GO:0032075)
negative regulation of growth (GO:0045926)
BHAT_ESR1_TARGETS_NOT_VIA_AKT1_DN
BHAT_ESR1_TARGETS_NOT_VIA_AKT1_UP
mitotic cell cycle (GO:0000278)
Cluster 1 2 3 4
-log10(FDR)

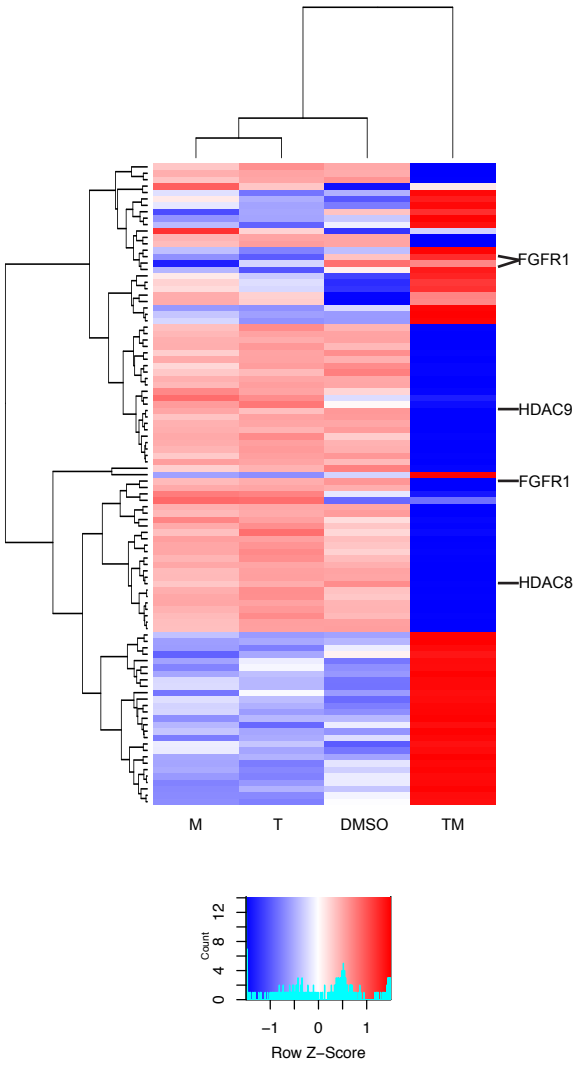
FGFR1
HDAC9
FGFR1
HDAC8
M
T
DMSO
TM
Count
0
4
8
12
−1
0
1
Row Z−Score

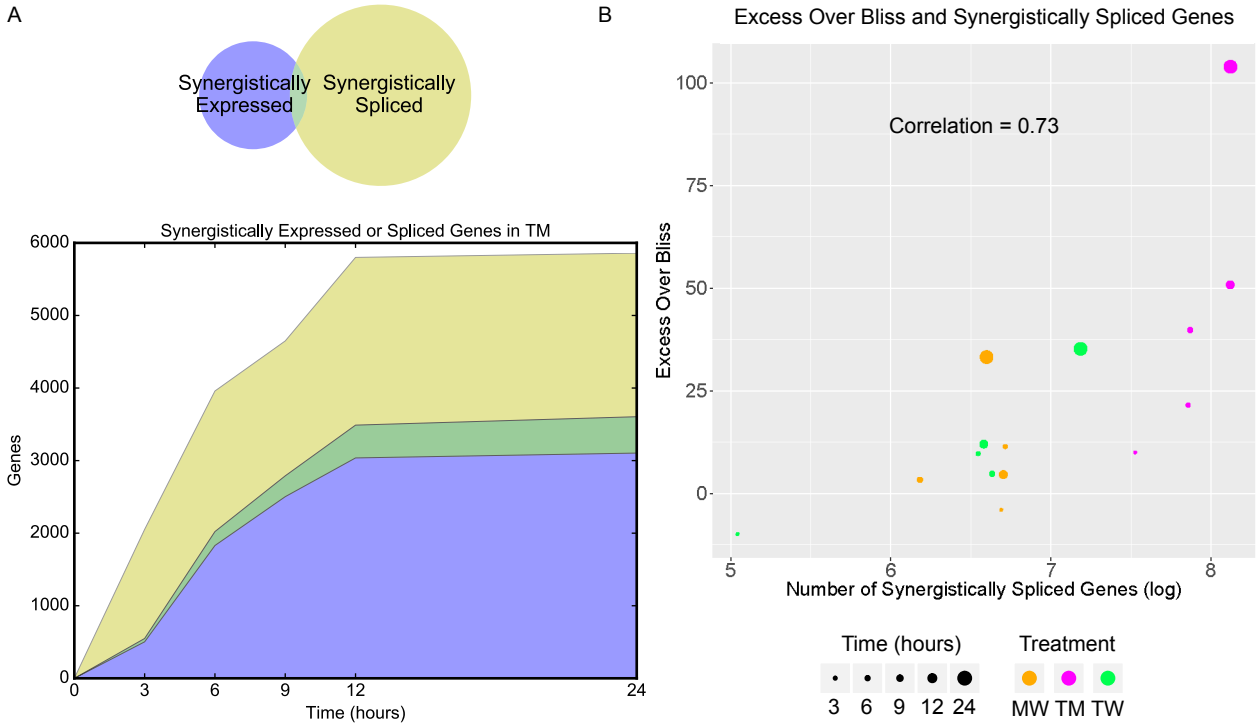
A
Synergistically Expressed
Synergistically Spliced
Synergistically Expressed or Spliced Genes in TM
Genes
Time (hours)
B
Excess Over Bliss and Synergistically Spliced Genes
Correlation = 0.73
Excess Over Bliss
Number of Synergistically Spliced Genes (log)
Time (hours)
3 6 9 12 24
Treatment
MW TM TW

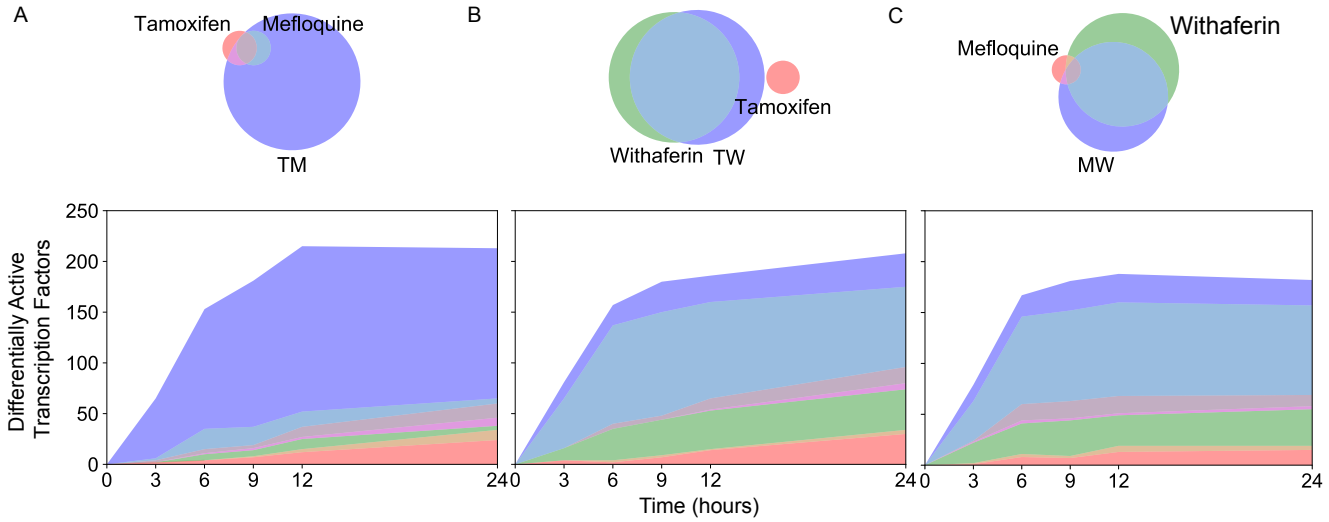
A
Tamoxifen
Mefloquine
TM
B
Tamoxifen
Withaferin
TW
C
Mefloquine
Withaferin
MW
Differentially Active Transcription Factors
250
200
150
100
50
0
0
3
6
9
12
24
Time (hours)

A

Tamoxifen Concentration	Drug 2 (Concentration)	Combination Index		
		12 hours	24 hours	48 hours
20.00 μM	Mefloquine (10.00 μM)	0.73	0.61	0.23
	Withaferin (4.96 μM)	2.38	0.72	NA

B

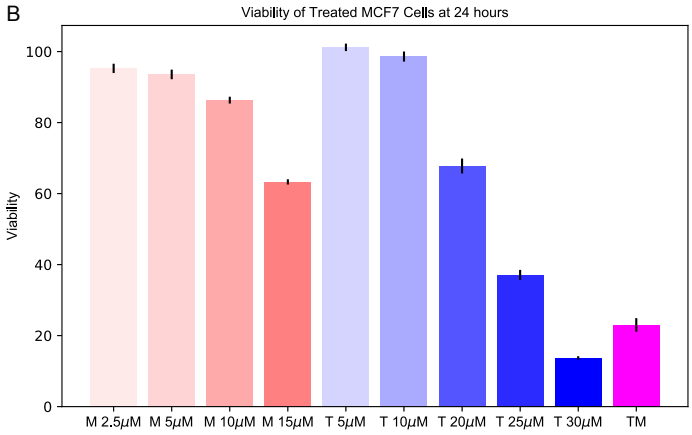

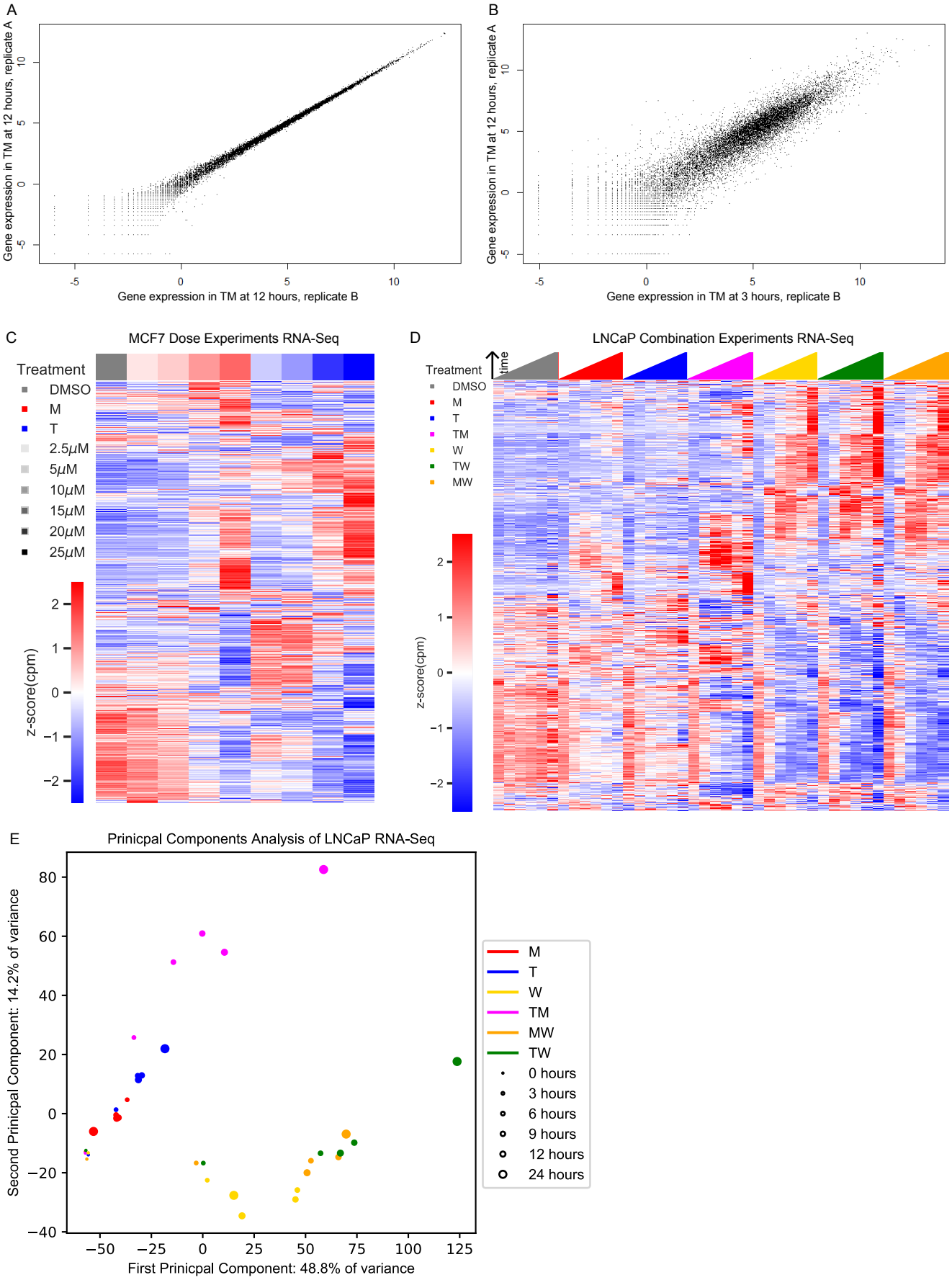
A
Gene expression in TM at 12 hours, replicate A
Gene expression in TM at 12 hours, replicate B
B
Gene expression in TM at 12 hours, replicate A
Gene expression in TM at 3 hours, replicate B
C
MCF7 Dose Experiments RNA-Seq
Treatment
DMSO
M
T
2.5μM
5μM
10μM
15μM
20μM
25μM
z-score(cpm)
D
LNCaP Combination Experiments RNA-Seq
time
Treatment
DMSO
M
T
TM
W
TW
MW
z-score(cpm)
E
Prinicpal Components Analysis of LNCaP RNA-Seq
Second Prinicpal Component: 14.2% of variance
First Prinicpal Component: 48.8% of variance
M
T
W
TM
MW
TW
0 hours
3 hours
6 hours
9 hours
12 hours
24 hours

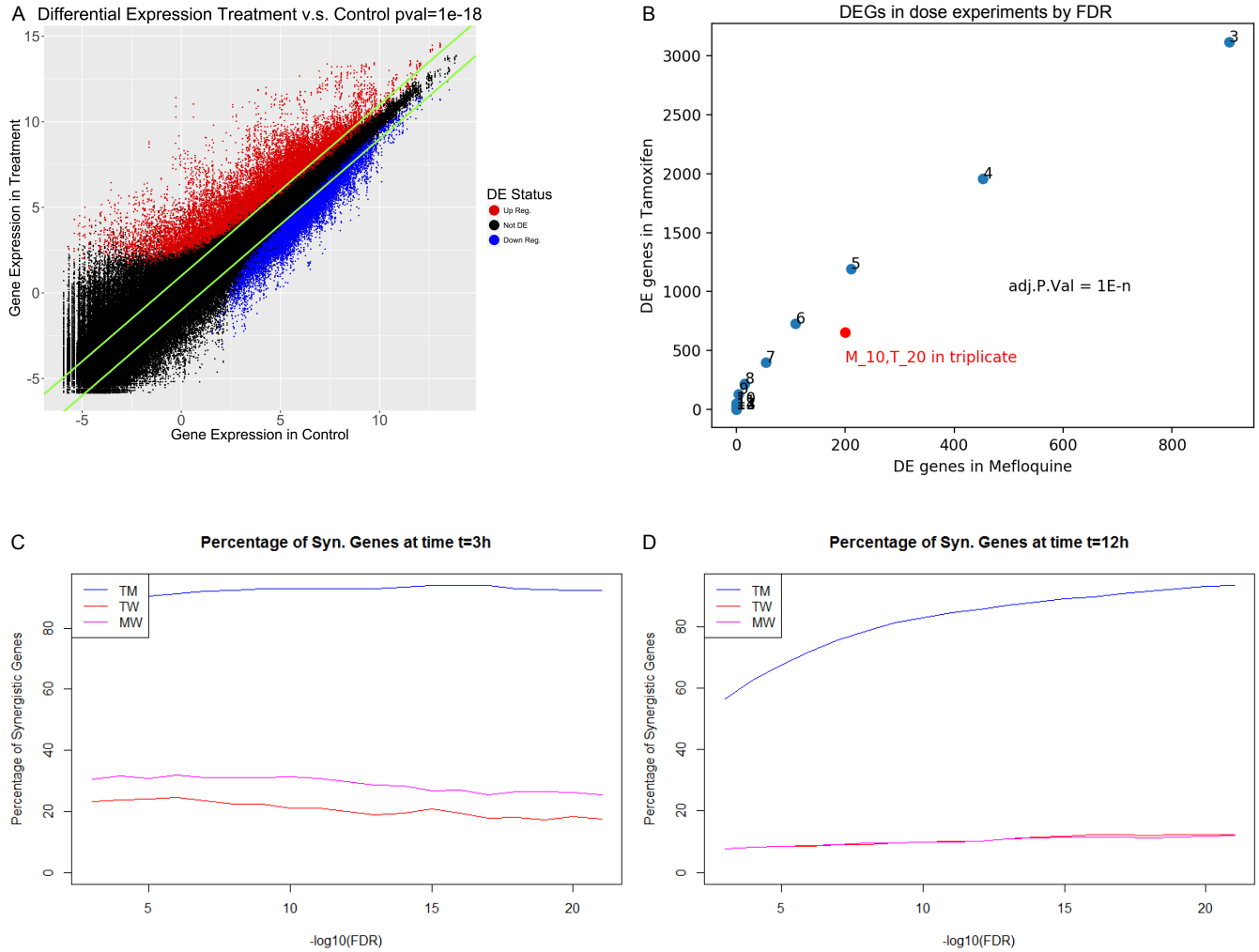
A
Differential Expression Treatment v.s. Control pval=1e-18
Gene Expression in Treatment
Gene Expression in Control
DE Status
Up Reg.
Not DE
Down Reg.
B
DEGs in dose experiments by FDR
DE genes in Tamoxifen
DE genes in Mefloquine
adj.P.Val = 1E-n
M_10,T_20 in triplicate
C
Percentage of Syn. Genes at time t=3h
Percentage of Synergistic Genes
-log10(FDR)
TM
TW
MW
D
Percentage of Syn. Genes at time t=12h
Percentage of Synergistic Genes
-log10(FDR)
TM
TW
MW

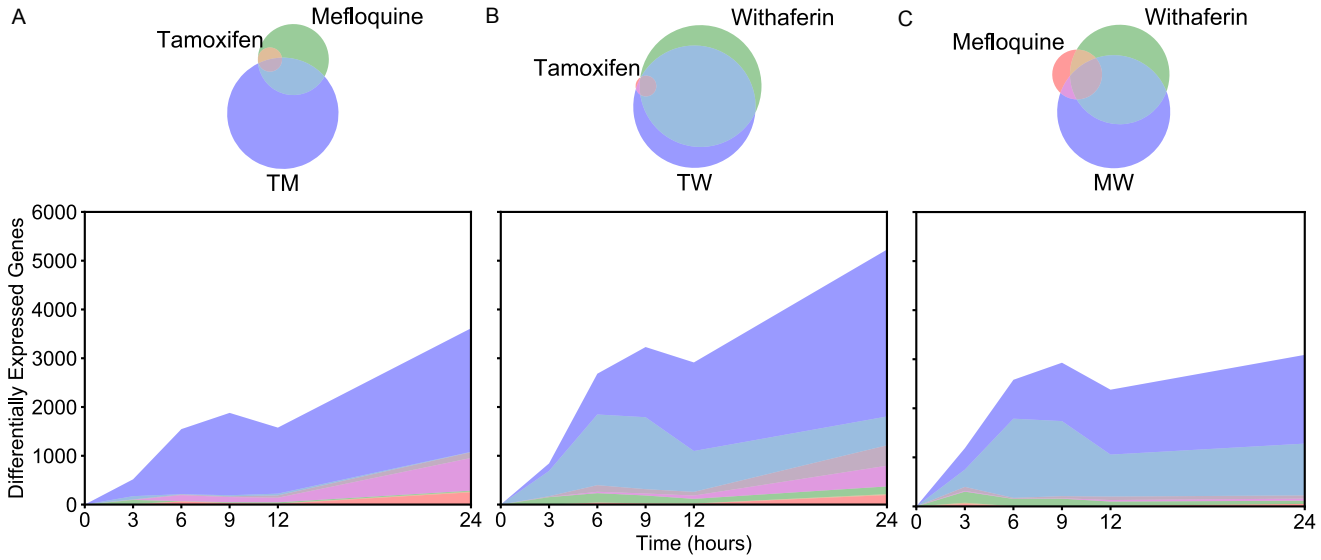
A
Mefloquine
Tamoxifen
TM
B
Withaferin
Tamoxifen
TW
C
Withaferin
Mefloquine
MW
Differentially Expressed Genes
6000
5000
4000
3000
2000
1000
0
0
3
6
9
12
24
Time (hours)

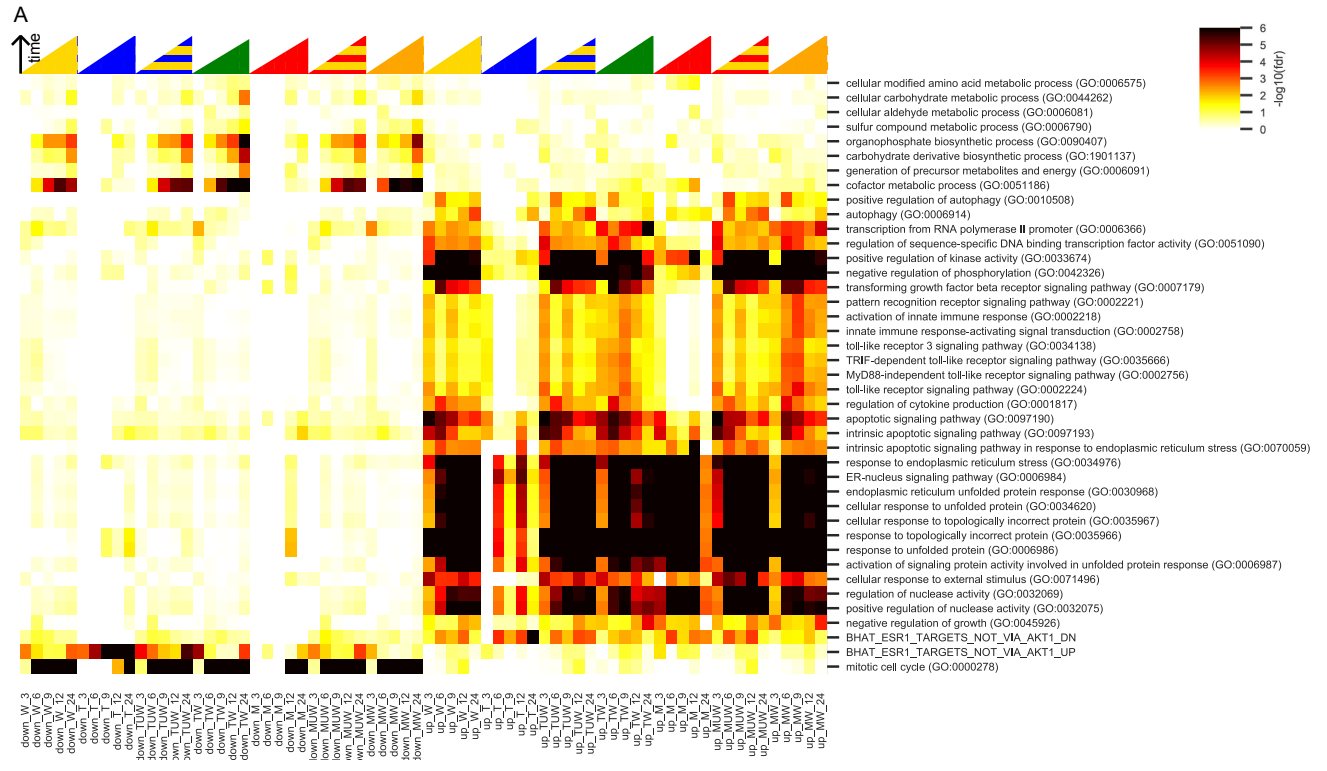
A
time
-log10(fdr)
6
5
4
3
2
1
0
cellular modified amino acid metabolic process (GO:0006575)
cellular carbohydrate metabolic process (GO:0044262)
cellular aldehyde metabolic process (GO:0006081)
sulfur compound metabolic process (GO:0006790)
organophosphate biosynthetic process (GO:0090407)
carbohydrate derivative biosynthetic process (GO:1901137)
generation of precursor metabolites and energy (GO:0006091)
cofactor metabolic process (GO:0051186)
positive regulation of autophagy (GO:0010508)
autophagy (GO:0006914)
transcription from RNA polymerase II promoter (GO:0006366)
regulation of sequence-specific DNA binding transcription factor activity (GO:0051090)
positive regulation of kinase activity (GO:0033674)
negative regulation of phosphorylation (GO:0042326)
transforming growth factor beta receptor signaling pathway (GO:0007179)
pattern recognition receptor signaling pathway (GO:0002221)
activation of innate immune response (GO:0002218)
innate immune response-activating signal transduction (GO:0002758)
toll-like receptor 3 signaling pathway (GO:0034138)
TRIF-dependent toll-like receptor signaling pathway (GO:0035666)
MyD88-independent toll-like receptor signaling pathway (GO:0002756)
toll-like receptor signaling pathway (GO:0002224)
regulation of cytokine production (GO:0001817)
apoptotic signaling pathway (GO:0097190)
intrinsic apoptotic signaling pathway (GO:0097193)
intrinsic apoptotic signaling pathway in response to endoplasmic reticulum stress (GO:0070059)
response to endoplasmic reticulum stress (GO:0034976)
ER-nucleus signaling pathway (GO:0006984)
endoplasmic reticulum unfolded protein response (GO:0030968)
cellular response to unfolded protein (GO:0034620)
cellular response to topologically incorrect protein (GO:0035967)
response to topologically incorrect protein (GO:0035966)
response to unfolded protein (GO:0006986)
activation of signaling protein activity involved in unfolded protein response (GO:0006987)
cellular response to external stimulus (GO:0071496)
regulation of nuclease activity (GO:0032069)
positive regulation of nuclease activity (GO:0032075)
negative regulation of growth (GO:0045926)
BHAT_ESR1_TARGETS_NOT_VIA_AKT1_DN
BHAT_ESR1_TARGETS_NOT_VIA_AKT1_UP
mitotic cell cycle (GO:0000278)

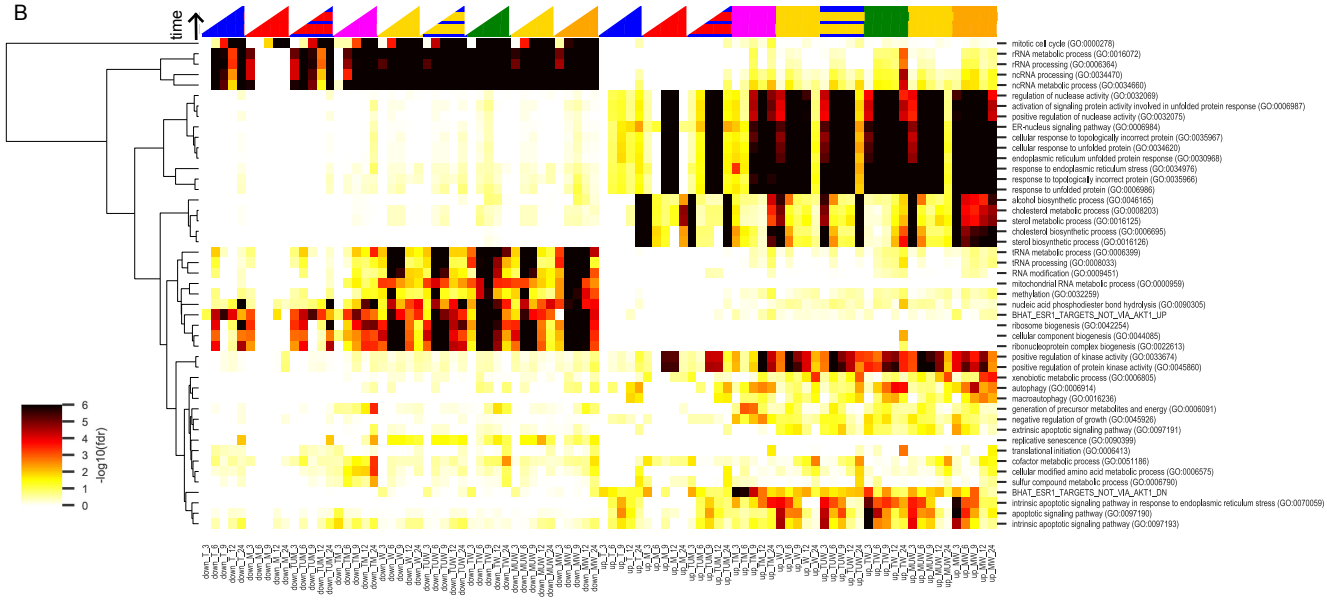
B
time
-log10(fdr)
6
5
4
3
2
1
0
mitotic cell cycle (GO:0000278)
rRNA metabolic process (GO:0016072)
rRNA processing (GO:0006364)
ncRNA processing (GO:0034470)
ncRNA metabolic process (GO:0034660)
regulation of nuclease activity (GO:0032069)
activation of signaling protein activity involved in unfolded protein response (GO:0006987)
positive regulation of nuclease activity (GO:0032075)
ER-nucleus signaling pathway (GO:0006984)
cellular response to topologically incorrect protein (GO:0035967)
cellular response to unfolded protein (GO:0034620)
endoplasmic reticulum unfolded protein response (GO:0030968)
response to endoplasmic reticulum stress (GO:0034976)
response to topologically incorrect protein (GO:0035966)
response to unfolded protein (GO:0006986)
alcohol biosynthetic process (GO:0046165)
cholesterol metabolic process (GO:0008203)
sterol metabolic process (GO:0016125)
cholesterol biosynthetic process (GO:0006695)
sterol biosynthetic process (GO:0016126)
tRNA metabolic process (GO:0006399)
tRNA processing (GO:0008033)
RNA modification (GO:0009451)
mitochondrial RNA metabolic process (GO:0000959)
methylation (GO:0032259)
nucleic acid phosphodiester bond hydrolysis (GO:0090305)
BHAT_ESR1_TARGETS_NOT_VIA_AKT1_UP
ribosome biogenesis (GO:0042254)
cellular component biogenesis (GO:0044085)
ribonucleoprotein complex biogenesis (GO:0022613)
positive regulation of kinase activity (GO:0033674)
positive regulation of protein kinase activity (GO:0045860)
xenobiotic metabolic process (GO:0006805)
autophagy (GO:0006914)
macroautophagy (GO:0016236)
generation of precursor metabolites and energy (GO:0006091)
negative regulation of growth (GO:0045926)
extrinsic apoptotic signaling pathway (GO:0097191)
replicative senescence (GO:0090399)
translational initiation (GO:0006413)
cofactor metabolic process (GO:0051186)
cellular modified amino acid metabolic process (GO:0006575)
sulfur compound metabolic process (GO:0006790)
BHAT_ESR1_TARGETS_NOT_VIA_AKT1_DN
intrinsic apoptotic signaling pathway in response to endoplasmic reticulum stress (GO:0070059)
apoptotic signaling pathway (GO:0097190)
intrinsic apoptotic signaling pathway (GO:0097193)

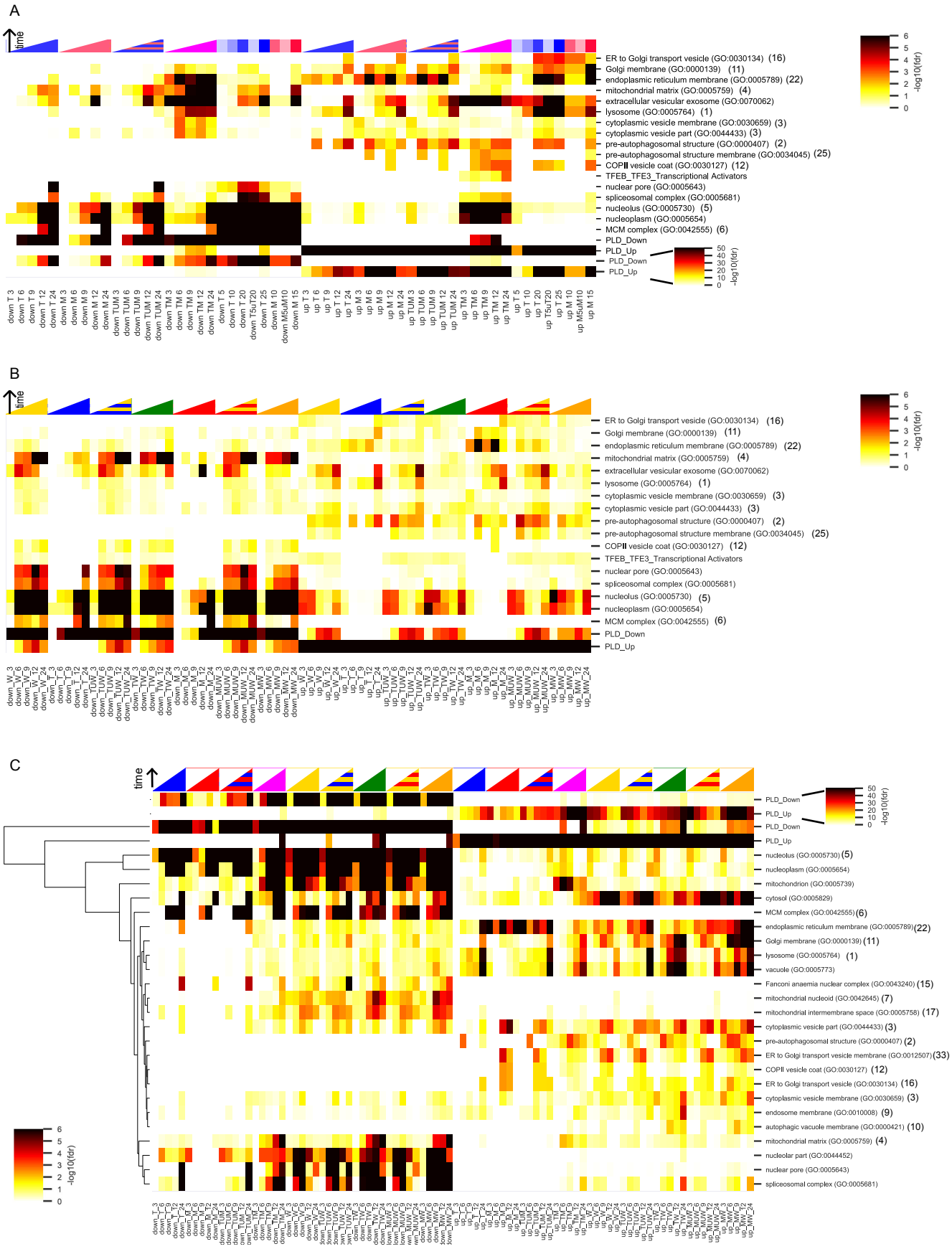
A
time
ER to Golgi transport vesicle (GO:0030134) (16)
Golgi membrane (GO:0000139) (11)
endoplasmic reticulum membrane (GO:0005789) (22)
mitochondrial matrix (GO:0005759) (4)
extracellular vesicular exosome (GO:0070062)
lysosome (GO:0005764) (1)
cytoplasmic vesicle membrane (GO:0030659) (3)
cytoplasmic vesicle part (GO:0044433) (3)
pre-autophagosomal structure (GO:0000407) (2)
pre-autophagosomal structure membrane (GO:0034045) (25)
COPII vesicle coat (GO:0030127) (12)
TFEB_TFE3_Transcriptional Activators
nuclear pore (GO:0005643)
spliceosomal complex (GO:0005681)
nucleolus (GO:0005730) (5)
nucleoplasm (GO:0005654)
MCM complex (GO:0042555) (6)
PLD_Down
PLD_Up
PLD_Down
PLD_Up
-log10(fdr)
B
time
ER to Golgi transport vesicle (GO:0030134) (16)
Golgi membrane (GO:0000139) (11)
endoplasmic reticulum membrane (GO:0005789) (22)
mitochondrial matrix (GO:0005759) (4)
extracellular vesicular exosome (GO:0070062)
lysosome (GO:0005764) (1)
cytoplasmic vesicle membrane (GO:0030659) (3)
cytoplasmic vesicle part (GO:0044433) (3)
pre-autophagosomal structure (GO:0000407) (2)
pre-autophagosomal structure membrane (GO:0034045) (25)
COPII vesicle coat (GO:0030127) (12)
TFEB_TFE3_Transcriptional Activators
nuclear pore (GO:0005643)
spliceosomal complex (GO:0005681)
nucleolus (GO:0005730) (5)
nucleoplasm (GO:0005654)
MCM complex (GO:0042555) (6)
PLD_Down
PLD_Up
-log10(fdr)
C
time
PLD_Down
PLD_Up
PLD_Down
PLD_Up
nucleolus (GO:0005730) (5)
nucleoplasm (GO:0005654)
mitochondrion (GO:0005739)
cytosol (GO:0005829)
MCM complex (GO:0042555) (6)
endoplasmic reticulum membrane (GO:0005789) (22)
Golgi membrane (GO:0000139) (11)
lysosome (GO:0005764) (1)
vacuole (GO:0005773)
Fanconi anaemia nuclear complex (GO:0043240) (15)
mitochondrial nucleoid (GO:0042645) (7)
mitochondrial intermembrane space (GO:0005758) (17)
cytoplasmic vesicle part (GO:0044433) (3)
pre-autophagosomal structure (GO:0000407) (2)
ER to Golgi transport vesicle membrane (GO:0012507) (33)
COPII vesicle coat (GO:0030127) (12)
ER to Golgi transport vesicle (GO:0030134) (16)
cytoplasmic vesicle membrane (GO:0030659) (3)
endosome membrane (GO:0010008) (9)
autophagic vacuole membrane (GO:0000421) (10)
mitochondrial matrix (GO:0005759) (4)
nucleolar part (GO:0044452)
nuclear pore (GO:0005643)
spliceosomal complex (GO:0005681)
-log10(fdr)

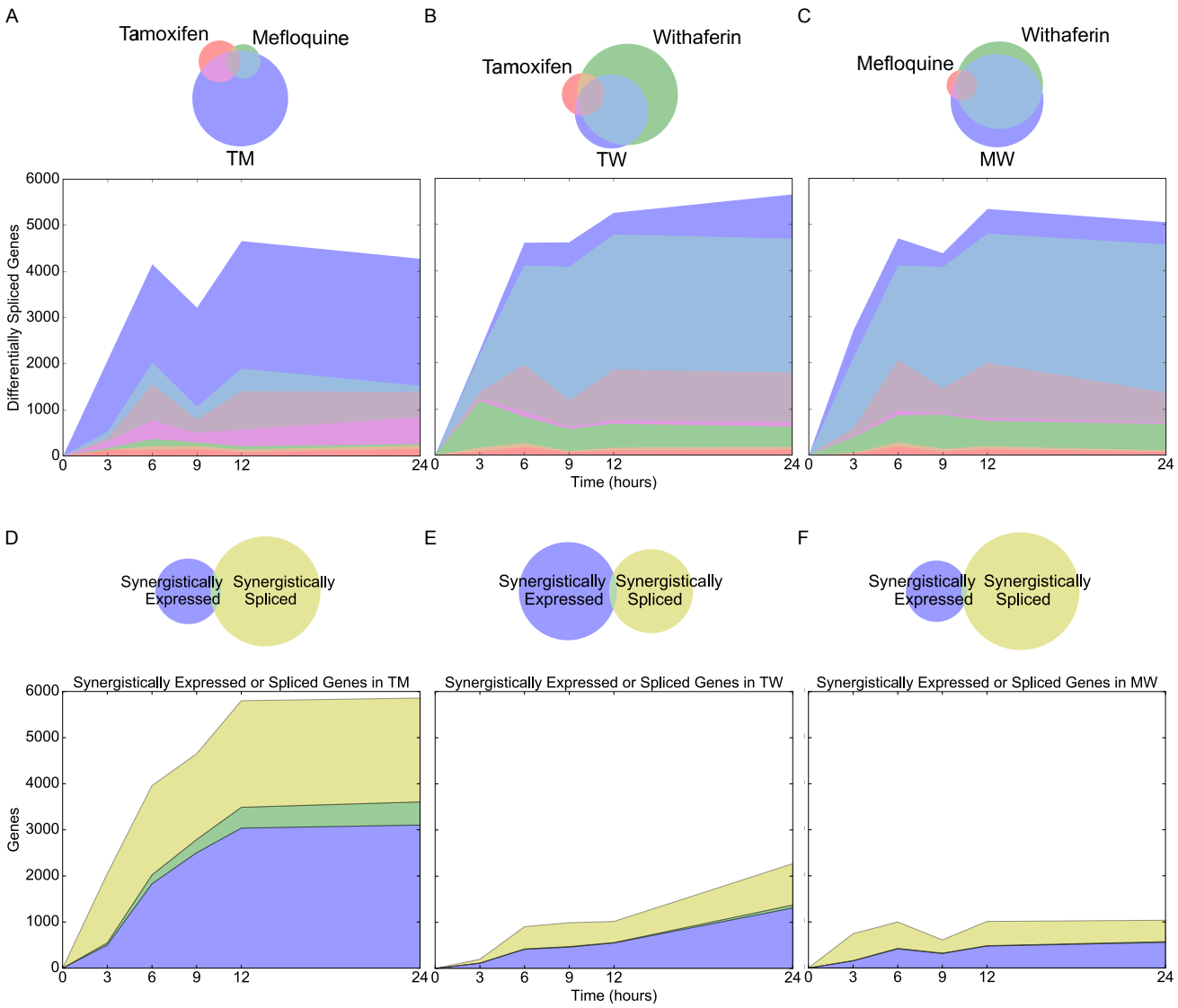
A
Tamoxifen
Mefloquine
TM
B
Tamoxifen
Withaferin
TW
C
Mefloquine
Withaferin
MW
Differentially Spliced Genes
6000
5000
4000
3000
2000
1000
0
0
3
6
9
12
24
Time (hours)
D
Synergistically Expressed
Synergistically Spliced
E
Synergistically Expressed
Synergistically Spliced
F
Synergistically Expressed
Synergistically Spliced
Synergistically Expressed or Spliced Genes in TM
Synergistically Expressed or Spliced Genes in TW
Synergistically Expressed or Spliced Genes in MW
Genes
Time (hours)